Accepted Manuscript

Measure Projection Analysis: A Probabilistic Approach to EEG Source Comparison and Multi-Subject Inference

Nima Bigdely-Shamlo, Tim Mullen, Kenneth Kreutz-Delgado, Scott Makeig

Measure Projection Analysis: A Probabilistic Approach to EEG Source Comparison and Multi-Subject Inference

Nima Bigdely-Shamlo,[a,b1] Tim Mullen,[a,c] Kenneth Kreutz-Delgado,[a,b] Scott Makeig[a]

[a] Swartz Center for Computational Neuroscience, Institute for Neural Computation,
University of California San Diego, La Jolla CA 92093-0559, USA
[b] Department of Electrical and Computer Engineering, University of California San Diego, La Jolla CA, USA
[c] Department of Cognitive Science, University of California San Diego, La Jolla CA, USA

Abstract

A crucial question for the analysis of multi-subject and/or multi-session electroencephalographic (EEG) data is how to combine information across multiple recordings from different subjects and/or sessions, each associated with its own set of source processes and scalp projections. Here we introduce a novel statistical method for characterizing the spatial consistency of EEG dynamics across a set of data records. Measure Projection Analysis (MPA) first finds voxels in a common template brain space at which a given dynamic measure is consistent across nearby source locations, then computes local-mean EEG measure values for this voxel subspace using a statistical model of source localization error and between-subject anatomical variation. Finally, clustering the mean measure voxel values in this locally consistent brain subspace finds brain spatial domains exhibiting distinguishable measure features and provides 3-D maps plus statistical significance estimates for each EEG measure of interest. Applied to sufficient high-quality data, the scalp projections of many maximally independent component (IC) processes contributing to recorded high-density EEG data closely match the projection of a single equivalent dipole located in or near brain cortex. We demonstrate the application of MPA to a multi-subject EEG study decomposed using independent component analysis (ICA), compare the results to k-means IC clustering in EEGLAB (sccn.ucsd.edu/eeglab), and use surrogate data to test MPA robustness. A Measure Projection Toolbox (MPT) plug-in for EEGLAB is available for download (sccn.ucsd.edu/wiki/MPT). Together, MPA and ICA allow use of EEG as a 3-D cortical imaging modality with near-cm scale spatial resolution.

Key words: EEG; independent component analysis; ICA; Clustering; Group-ICA, Measure Projection Analysis

[1] Correspondence to: Nima Bigdely-Shamlo

E-mail: nima@sccn.ucsd.edu, Phone: +1 858-822-7538

1.1 Introduction

Because of the very broad biophysical point-spread function governing volume conduction of areal potentials generated in the human brain to scalp electrodes measuring their summed electroencephalographic (EEG) activity, proper analysis of event-related or ongoing EEG dynamics should best focus on EEG source activities and corresponding (3-D) brain source locations rather than on scalp channel activity records and (2-D) channel locations. Comparing 3-D source locations and source dynamics across subjects and sessions of an EEG study is, however, more difficult that simply equating scalp channel locations across subject and sessions, as is typical in EEG studies that analyze the scalp channel signals directly.

Here we introduce a probabilistic approach, Measure Projection Analysis (MPA), for population-level inference from source-resolved EEG signals. This approach provides, for each EEG measure of interest, 3-D maps of separable brain domains with separable source measures plus statistical estimates of measure differences across group and/or conditions. Although source-level locations and dynamics used in MPA might be derived from any EEG source discovery method, e.g., beamforming or trial-averaged event-related potential (ERP) source analysis, we here demonstrate its application to an example EEG study decomposed using independent component analysis (ICA) and compare its results to those of the PCA-based independent component (IC) clustering available in EEGLAB (Delorme & Makeig, 2004).

ICA (Bell and Sejnowski, 1995) has become a method of widespread interest for analysis of EEG data (Makeig et al., 1996), (Makeig et al., 1997), (Lee et al., 1999), (Jung et al., 2001), (Makeig et al., 2002). In this approach to EEG source analysis, unaveraged continuous or epoched EEG data from multiple scalp channels are decomposed into independent component (IC) processes by learning a set of spatial filters that have fixed relative projections to the recording electrodes and produce maximally independent individual time courses from the data. ICA thus learns *what* independent processes (information sources) contribute to the data and also reveals their individual scalp projection patterns (scalp maps), thereby simplifying the EEG inverse source localization problem to that of estimating *where* each source is generated, a much simpler problem than estimating the source distributions of their ever-varying linear mixtures as recorded by the scalp electrodes themselves.

The IC filters linearly transform the representational basis of EEG data from a channel matrix (scalp channels by time points) to a sum of independent component processes with maximally independent time courses and fixed scalp projections (scalp maps, with often strongly overlapping topographies). Many ICs predominately account for the contributions to the channel data from a non-brain ('artifactual') source process -- for example potentials arising from eye movements, scalp muscle activity, the electrocardiogram, line noise, etc., while many other ICs are compatible with a source within the brain itself, in particular within its convoluted cortical

2

shell in which most of the spatially organized potentials reaching the scalp are generated (Nunez and Srinivasan, 2006).

Many of the brain-based ('non-artifactual') IC scalp topographies may be modeled as the projection of a single equivalent dipole inside the brain volume (Makeig et al., 2002). ICA algorithms return many such 'dipolar' IC data sources (those for which most of the spatial variance of the electric field pattern they produce on the scalp is accounted for by the projection of a single 'equivalent' dipole). On average, the more independent the resulting ICs returned by an linear ICA decomposition method, the more near-dipolar ICs are returned (Delorme et al., 2012). Such dipolar ICs are compatible with an origin in locally-synchronous cortical field activity within a single cortical patch, which by biophysics must be located near to and oriented predominantly perpendicular to the equivalent dipole (Scherg, 1990) (A few clearly brain-based ICs may have scalp maps very closely resembling the summed projection of two bilateral cortical patches that contribute synchronous activity to the scalp signals).

Finding the actual cortical patch (or patches) generating a given dipolar IC may be difficult (Acar et al., 2009), as it requires (at least) a good quality MR head image for the subject and accurately recorded scalp electrode positions (Acar and Makeig, 2010). Given a good estimate of where the scalp electrodes were placed on the head, and a near-dipolar IC scalp map, the location of the equivalent dipole may be found reliably, in many cases with less than a centimeter error when 3-D electrode positions are recorded (Akalin Acar, submitted) and an accurate skull conductance value is used in the analysis. Biophysical simulations also show that the equivalent dipole for a cm^2-scale cortical patch source is, on average, less than 2 mm from the center of the generating patch (Akalin Acar, unpublished). Thus, a unique advantage of ICA applied to EEG is that localizing sources from its single-source IC scalp maps avoids uncertainties associated with multiple local minima that limit the accuracy of estimates of the more complex source distributions computed from scalp maps that sum projections of multiple sources -- for example nearly all raw EEG scalp maps or maps for later peak latencies in ERP waveforms. Of course this level of spatial accuracy is only possible using single-subject head models, which are possible only when an MRI head image is available (as it was not for our subjects). Using individual head models for localization will make it necessary to warp the cortical locations of the multiple subjects into a common head model to allow group Measure Projection. Results calculated, as here, using IC locations in a common head model may well have somewhat less spatial accuracy, though their accuracy might be improved in subject-level analysis by translating them back to associated locations in individual subject head models, including models constructed by warping a common template model to the recorded 3-D positions of the scalp electrodes (Acar and Makeig, 2010). However, unless subjects are highly ethnographically diverse (infants and adults, for example) the choice of head model is unlikely to have much effect on the topology of the MPA results -- more anterior source domains will remain more anterior, etc.

Since ICA uses waveform differences to separate independent sources, which depend both on the exact placements of the scalp electrodes and the individual subject cortical geography, optimal separation is achieved when it is applied to data channels recorded simultaneously from a single subject with a single scalp montage. The length of the training data must be sufficient for the number of recording channels. Since both EEG channel locations and conductance values slightly differ across subjects and sessions, and positions and orientations of corresponding cortical source areas differ across subjects, ICA decompositions are best applied separately to each recorded session or smaller data set from a single recording session.

A standard way to analyze EEG data is to first conduct an experiment in which a number of (outwardly) similar events occur, typically stimulus (e.g., image) presentation and behavioral events (e.g., impulsive button presses). Sets of EEG activity epochs recorded in some latency window around these events (experimental trial epochs) are extracted, averaged, and compared. A number of mean measures of event-related EEG trial data have been developed in recent years and incorporated into freely available software toolboxes including EEGLAB (Delorme and Makeig, 2004), Fieldtrip (Oostenveld et al., 2011), the SPM toolkit (Friston, 2007), and ICALAB (Cichocki and Amari, 2002). These measures, including average ERP time series and event-related spectral perturbation (ERSP) (Makeig, 1993) and inter-trial coherence (ITC) time/frequency transforms, may equally be computed for single ICs as well as for single scalp channels. For each subject session and associated ICA decomposition, each IC has a unique scalp map and EEG time course. To support group-level inferences about EEG measure differences across task trial conditions, subject groups, recording sessions, etc., IC location and EEG measure information must be integrated across subjects and sessions

In contrast to the common approach to obtaining group inferences from channel data, i.e. by assuming equivalence across subjects of electrode derivations from standardized scalp locations (Picton et al., 2000) (Kiebel and Friston, 2004), combining results across different ICA decompositions is non-trivial. Several methods have been proposed for this task. These typically fit into two categories: IC clustering (Makeig et al., 2002), (Onton et al., 2006), (Onton and Makeig, 2006) , (Spadone et al., 2012) and joint decomposition methods such as group-ICA (Eichele et al., 2009), (Kovacevic and McIntosh, 2007), (Calhoun et al., 2009), (Congedo et al., 2010), multi-set canonical correlation analysis (Li et al., 2009) and J-BSS (Li et al., 2011) (Via et al., 2011) .

Although the IC clustering method uses a potentially larger subspace of the signal (involving less dimensionality reduction than most joint decomposition methods) and poses fewer restrictive assumptions regarding the relationship between signal sources at subject and group level, it often involves tuning multiple parameters (relative measure weights, number of cluster, etc..), potentially reducing the objectivity of the analysis and reproducibility of the results; for a recent

approach to tackling this problem see (Spadone et al., 2012). Also, it is often impractical to calculate the significance of IC clusters themselves, whose averages are often used in subsequent statistical tests for measure differences across conditions or groups.

MPA aims to solve the problem of comparing EEG source locations and dynamics across subjects and sessions in 3-D brain space using a probabilistic approach that treats the source-resolved data as samples drawn from the distribution of source locations and dynamics. By performing statistical comparisons on a grid of brain locations instead of individual sources, and focusing on a single dynamic measure of interest at a time, MPA reduces the number of parameters assumed in the analysis, and delivers estimates of the statistical reliability of the results. Here we demonstrate the application of MPA by applying MPT tools to an example EEG study, comparing its results to standard PCA-based IC clustering, and studying the robustness of the MPA results using surrogate data.

1.2 Methods

The Measure Projection Analysis (MPA) approach introduced here comprises four steps: 1) After decomposition of the unaveraged EEG data by ICA into brain source processes (ICs), the location of each source signal used in the analysis is computed within a common brain template model, here in the form of a IC source equivalent dipole. 2) Spatial smoothing of a given dynamic measure for the equivalent dipole-localized ICs is performed using a truncated 3-D Gaussian spatial kernel; 3) A subspace of brain voxel locations with significant local IC measure similarity are identified (see Appendix A for a detailed description); 4) Spatial brain voxel domains within the measure similarity subspace that exhibit sufficient measure differences are identified using affinity clustering (details in Appendix B).

1.2.1 Experimental data

EEG data were collected from 128 scalp locations at a sampling rate of 256 Hz using a Biosemi (Amsterdam) Active View 2 system and a whole-head elastic electrode cap (E-Cap, Inc.) forming a custom, near-uniform montage across the scalp, neck, and bony parts of the upper face.

====== **Figure 1 here** =======

1.2.2 Subject task

Our sample study consisted of data from 15 sessions recorded from 8 subjects performing a Rapid Serial Visual Presentation (RSVP) task (Bigdely-Shamlo et al., 2008) (the raw data are available at ftp://sccn.ucsd.edu/pub/headit/RSVP, the EEGLAB Study files at ftp://sccn.ucsd.edu/pub/measure_projection/rsvp_study). Each session comprised 504 4.9-s image bursts of 49 oval image clips from a large satellite image of London presented at a rate of

12/s. Some (60%) of these bursts contained one image in which a target white airplane shape was introduced at a random position and orientation. Following each burst, subjects were asked to press one of two buttons to indicate whether or not they had detected a target airplane in the burst. Fig 1 shows a time-line of each RSVP burst. For further details see (Bigdely-Shamlo et al., 2008).

1.2.3 Data preprocessing.
After preprocessing each subject data set using EEGLAB (sccn.ucsd.edu/eeglab) and custom Matlab functions for re-referencing, from the active-reference Biosemi EEG data to an electrode over the right mastoid, high-pass filtering above 2 Hz, and rejection of channels and data containing non-stereotypical artifact, an ICA decomposition was performed for each recording session. The subset of ICs that could be represented by an equivalent dipole model with low error (here defined as more than 85% of channel variance in the IC scalp map being accounted for by a single equivalent dipole or in a few cases a bilaterally symmetric equivalent dipole pair) were selected for analysis. ICs with equivalent dipoles located outside the MNI brain volume (e.g., those with an minimum distance to the MNI brain surface larger than 1 mm) were removed as artifactual, and mean event-related power spectral perturbations (ERSPs) to target and Nontarget images were computed for the remaining 260 ICs (per session mean 18, standard deviation ± 8).

1.2.4 ERSP measure projection
Fig. 2A represents the processing pipeline schematically. To apply MPA to the RSVP study we used a Measure Projection Toolbox (MPT) for MATLAB (The Mathworks, Inc.) implementing MPA and operating as an EEGLAB plug-in (freely available for download at sccn.ucsd.edu/wiki/MPT). To compare MPA results to those of IC clustering as implemented in EEGLAB, we set the standard deviation of the three-dimensional Gaussian representing each equivalent dipole location probability density to 12 mm. This parameter reflected a heuristic estimation of the combined ambiguity in equivalent dipole locations arising from a) numerical inaccuracies in the IC component maps, b) errors in co-registering the measured channel locations with the standard brain model, c) inaccuracies in the forward head model, d) particularly in assumed conductances of skull and brain tissues, and e) difference across subjects in brain locations of functionally equivalent brain areas. This standard deviation value was also chosen in part to produce smoother spatial distributions for this rather small EEG study: for larger studies it might be usefully reduced. We truncated each Gaussian to a radius of 3 standard deviations (36 mm) to prevent spurious influences from distant dipoles in sparsely filled source regions.

Brain model: A cubic dipole source space grid with 8-mm spacing (3,908 vertices) was situated in the brain volume in MNI space. Voxels outside the MNI brain volume were excluded. Local convergence values (see Appendix A for definition) were calculated using Eq. (A.2), A pairwise

IC similarity matrix was constructed by estimating the signed mutual information between IC-pair ERSP measure vectors using a Gaussian distribution assumption (Darbellay and Vajda, 1999):

$$\text{Mutual Information} = \frac{1}{2}\,\text{sign}\,(\text{correlation})\,\log_2\left(\frac{1}{1-\text{correlation}^2}\right)\,(\text{bits}/\text{sample}) \quad (1)$$

The reason for using an estimate of signed mutual information instead of correlation itself was because equal correlation intervals may reflect unequal information differences. For example, the difference in mutual information values associated with IC measure correlation values of 0.8 and 0.9 is far greater than mutual information difference associated with IC correlations of 0.1 and 0.2. In addition, mutual information values (in bits/sample) may be meaningfully averaged. In switching to use of signed estimated mutual information instead of linear correlation, we also observed an improvement in the spatial smoothness of the obtained MPA significance values.

A significance threshold for convergence values at each brain grid location was obtained by bootstrap statistics. We permuted the similarity matrix (with substitution), in effect removing the correspondence between each IC and its associated ERSP, and calculated 2,000 surrogate convergence values at each voxel associated with the null hypothesis of no stable association between brain region and ERSP. Probability values were calculated by finding the percentage of bootstrap convergence values larger than the original convergence value (right-tail comparison).

A group-wise $p < 0.05$ threshold, corrected for multiple comparisons using False Discovery Rate (FDR) testing (Benjamini and Hochberg, 1995), gave a raw voxel significance threshold of $p < 0.0075$. Voxels with convergence probabilities lower than this threshold defined the ERSP 'measure convergence subspace' of brain voxel locations at which the local similarity of IC ERSPs was significantly higher than what could be expected by chance in these data.

Condition difference tests: For each identified study domain d and subject session s, statistical significance of differences between the Target and Non-Target condition ERSPs was computed by first projecting the ERSP associated with each condition c to each voxel i in the domain, producing projected measure $M(c,i,d)$. We then calculated a weighted-mean measure $W(d,s,c)$ across all v domain voxels, each weighted by $D(i,s)$, the dipole density of voxel i in session s, and then normalized by total domain voxel density.

$$W(d,s,c) = \frac{\sum_{i=1}^{v} M(c,i,d)D(i,s)}{\sum_{i=1}^{v} D(i,s)} \quad (2)$$

Where

$$D(i,s) = \sum_{j=1}^{n} P_j(i) \tag{3}$$

Above, n is the number of component dipoles in the session and $P_j(i)$ is the model probability that dipole j is actually at domain voxel i (see Appendix A).

Next, a two-tailed Student-T test was applied to the collection of session-mean projected measures in the two conditions to test for reliable domain-ERSP condition differences. For visualization, non-significant ($p \geq 0.05$) values in each domain condition-ERSP difference were masked by replacing them with 0s.

1.2.5 ERSP domain clustering

To simplify the analysis of projected source measure values in the measure convergence subspace, we separated them into several distinguishable spatial *domains* by threshold-based Affinity Propagation clustering (described in Appendix B) based on a similarity matrix of pair-wise correlations between the projected measure values at each voxel position. Affinity propagation automatically finds an appropriate number of clusters (below referred to as spatial domains) based on the maximum allowed correlation between cluster exemplars, automatically increasing the number of clusters until any other potential cluster exemplar becomes too similar to one of the existing exemplars. Here, maximal exemplar-pair similarity (forcing creation of additional clusters) was set to a correlation value of 0.8, and the outlier detection similarity threshold to a correlation value of 0.7. The method did not find any outlier voxels since all of the projected measures in each domain had a correlation with their domain exemplar higher than 0.7. The minimum correlation value is in fact an optional parameter: one could decide to not exclude any significant voxel from domain analysis by setting the minimum correlation threshold to negative infinity. Note that the voxel clustering procedure does not force the voxels within a single domain to be contiguous; for example near-identical ERSPs may be produced in bilaterally symmetric cortical regions, which may then be identified by affinity clustering as a single measure domain. Fig. 2A summarizes the MPA steps used to create distinguishable spatial source domains for each EEG measure.

====== **Figure 2 here** ======

1.2.6 PCA-based IC clustering

In the PCA-based IC clustering approach implemented in EEGLAB (Makeig et al., 2002; Onton & Makeig, 2006), cross-session IC equivalence classes are typically defined by applying a clustering algorithm such as k-means to an L2-weighted combination of EEG measures of interest (e.g., IC equivalent dipole locations, scalp-map topographies, mean power spectra, average ERPs, etc.) so as to produce a desired number of IC clusters (10-30). Cluster-level mean

EEG measure values may then be calculated by averaging across the members of each IC cluster, and may then be used for group-level inference and event or task condition comparison. The default IC clustering options create a *pre-clustering array* that represents each IC as positioned in a joint-measure feature space by the following operations:

- *Mean EEG measure computation:* For each IC, each set of experimental trials (experimental 'condition') and each EEG measure of interest (ERP, mean power spectrum, ERSP, and/or Inter-Trial Coherence (ITC)), subject-mean IC measure values are computed and then concatenated across conditions.

- *Measure dimensionality reduction:* Next, the dimensionality of the concatenated condition measures for each IC is reduced by PCA to a principal subspace. The subspace dimensionality is heuristically determined based on the amount of trial data available. Measure values associated with each IC in the PCA-reduced coordinates are normalized by dividing them by the standard deviation of the first principal component.

- *Equivalent dipole locations:* Dipole (x,y,z) location values in the adult template MNI brain space (Montreal Neurological Institute and Hospital, (Evans et al., 1993)) are normalized and then multiplied by a user-specified scalar weight to determine their relative influence in the subsequent clustering.

- *Joint-measure IC-space representation:* Dimensions associated with each EEG measure (after preprocessing steps describe above) are concatenated to represent each IC in a joint space. For example, ERSP information represented by 10 PCA dimensions may be concatenated with 5 PCA dimensions representing ERP information and 3 (MNI x,y,z) location dimensions representing dipole position to form a joint 10+5+3 = 18 dimensional space in which each IC is located.

- *IC clustering:* ICs in this joint-measure IC space are then clustered using *k*-means or some other clustering method. The number of clusters is user supplied.

All ICs, represented by features in the resulting pre-clustering array, are then clustered using the k-means method implemented in the Matlab Statistics Toolbox (The Mathworks, Inc.). Fig. 2B shows a flowchart of this clustering method. For more details and a sample application of this procedure, see (Onton and Makeig, 2006).

1.2.7 PCA-based ERSP measure clustering
EEGLAB default (PCA) clustering was used to create 15 clusters using ERSP and dipole location measures. ERSP values for Target and Nontarget conditions were concatenated across the time dimension for each IC and were reduced to 10 principal dimensions by PCA. After

default normalization, equivalent dipole location values were weighted by the default factor 10. The MATLAB implementation of the *k*-means method was then used to form IC clusters.

Clustering results for different numbers of clusters were first examined by eye and the number of clusters was thereby adjusted such that (a) dipoles assigned to a given cluster formed a single, relatively focal cluster, in anatomical (MNI) space (although it is possible for multiple distal brain regions to display similar EEG dynamics, resulting in clusters with dipoles localized to multiple brain regions, we have found that such clusters usually appear as a consequence of cluster merging when the number of clusters is set too low); and (b) clusters are maximally non-overlapping and contain a reasonable number of dipoles (overlapping and/or small-size clusters may occur when the number of clusters is either too low or too high). These criteria did not take into account the similarity structure of other measures (e.g., ERPs) which would ideally further influence the choice of cluster number.

1.3 Results

====== **Figure 3 here** ======

1.3.1 ERSP measures for PCA-based IC clusters
Fig. 3 shows a scatter-plot of computed IC-pair ERP and ERSP similarities. Because of the inherent ambiguity in the polarity of IC activations, absolute-value correlations of ERPs for each IC pair was used as an upper bound on their ERP similarity. As can be seen in this figure, as the correlation between these two sets of values is low (0.26), the similarity structures of (absolute) ERP and ERSP measures are far from identical. This affirms our decision here to not include ERP measure data in ERSP clustering.

====== **Figures 4 & 5 here** ======

Figures 4 and 5 show cluster dipole locations and Target ERSP values averaged over ICs belonging to each cluster. Fig. 4 shows a subset of clusters with large (more than 1.7-dB) mean Target ERSP values, while Fig. 5 shows clusters with mean Target ERSP values below 1.3 dB. Although most eye movement-related components were rejected as they were localized outside MNI brain volume, due to localization errors some of these IC were assigned to locations inside brain; these were concentrated in Cluster 11.

Nontarget ERSP values were lower ($p < 0.05$) or close to zero for all these clusters. Statistical significance analysis of differences between Target and Nontarget ERSPs was performed by bootstrap statistics permuting Target and Nontarget conditions across ICs belonging to each cluster. This statistical test was performed for each cluster separately.

====== **Figure 6 here** ======

1.3.2 ERSP measure projection results

Fig. 6A shows the significant voxels (p<0.0075; group-wise p < 0.05 under FDR). The voxels were colored by first applying non-metric multi-dimensional scaling (MDS, as implemented in Matlab *mdscale* function with stress normalized by the sum of squares of the interpoint distances and other parameters set to their default values) to the projected (concatenated Target and Nontarget) ERSP measures, by this means mapping them to a single dimension. These 1-D MDS values were then mapped to the [.00, .69] hue interval in the MATLAB hue color scale (from red to blue) so as to display brain locations with similar projected measures in similar colors. Fig. 6B shows four measure-consistent IC domains obtained from the Affinity Propagation method implemented as threshold-based clustering (Appendix B). These are colored by one-dimensional MDS of the projected measure associated with their most representative member (the domain exemplar, using a similar MDS procedure as in Fig. 6A). By comparing Figures 6A and 6B we can see how these four domains summarize the projected measure values: Fig. 6A shows roughly four colored regions that map into the four identified measure domains shown in Fig. 6B.

====== **Figure 7 here** ======

Fig. 7 shows an alternative visualization of ERSP Domains: exemplar MNI cortical surface is colored by domain color, weighted by dipole density, from brain-grid positions radially below each cortical location.

1.3.3 Comparison of MPA and PCA-based clustering methods

Next, we compared the results obtained from PCA-based IC clustering to those obtained using measure projection analysis (MPA).

====== **Table 1 here** ======

Table 1 gives the cluster number(s) located in or near each domain. Average ERSPs for these clusters are highly similar to those of respective domain exemplars, indicating that here measure projection analysis produced results in close agreement with IC clustering in locations with statistically significant ERSP similarity across subjects.

Our PCA-based clustering, on the other hand, gave 15 clusters, many not associated with any significantly convergent MPA region. For example, Clusters 2 and 3 in Fig. 5 are relatively far from brain areas with significant ERSP convergence shown in Fig. 6A. Since MPA showed that ICs associated with these PCA-based clusters have fairly dissimilar ERSP measures, there is not

11

much statistical evidence in the data for MPA spatial convergence in these regions to support the validity of these clusters.

Table 1 also lists anatomical locations associated with each ERSP domain based on the LONI project probabilistic atlas (Shattuck et al., 2008) and Brodmann areas (Brodmann, 1909) from (Lancaster et al., 2000). The listed functional associations of these areas are based on Brodmann's Interactive Atlas (fmriconsulting.com/brodmann/Introduction.html). On close inspection, because of errors in dipole localization related to insufficient electrical head modeling in the complex peri-orbital regions, many eye-artifact ICs (13 out of 16 highly contributing ICs) in this study were localized inside the brain volume and became the main contributors to ERSP Domain 1 and PCA Cluster 11. In measure projection analysis, brain and non-brain ICs should not be mixed. Performing an additional artifact IC rejection step, using methods for identifying eye artifact ICs from their activity profiles as well as their equivalent dipole locations such as CORRMAP (Viola et al., 2009) or ADJUST (Mognon et al., 2011) should be done before MPA to give meaningful results in frontal regions.

Of similar concern are ICs accounting for scalp muscle activity that, for EEG montages with sufficient scalp coverage, have scalp maps consistent with an equivalent dipole at the insertion of the muscle into the skull (as seen in(Onton et al., 2006)). These may be differentiated from brain ICs prior to measure projection by their dipole locations (outside the skull) and by their characteristic electromyographic (EMG) spectra with a minimum below 20 Hz and a high-level plateau at higher frequencies. Here we removed scalp/neck muscle ICs based on their dipole locations before applying measure projection.

Domains 2 and 3 are both associated with Secondary (V2), Associative (V3) and Primary (V1) visual cortex (BA 18,19 and 17) (Marcar et al., 2004) (Dougherty et al., 2003). Domain 3 is in or near BA 31 which has been reported to support high-demand visual processing and discrimination (Deary et al., 2004). Domain 2 is in or near bilateral BA 37 and fusiform gyrus (with a right bias), areas reported in a fMRI study of a visual perceptual decision-making task (Philiastides and Sajda, 2007). Similar low-theta band activity occurring about 400 ms after visual target detection in these brain areas was reported in (Makeig et al., 2004).

There is some evidence of mu rhythm desynchronization (suppression) in Domain 4, located in or near right-hand Primary Somatomotor, Primary Motor, and Somatosensory Association areas (BA 7,3,2,4), which may be related to mu rhythm activity that appears in hand somatomotor cortex when subjects hold a button in their right hand (Makeig et al., 2004). Subjects were asked to wait until the end of RSVP image burst before pressing a response button. The mu rhythm activity in this area is thought to reflect cortical inhibitory (or 'idling') dynamics that may decrease the chance of prematurely pressing the button. Activation in or near BA40 and BA7 is also consistent with a preliminary FMRI study conducted by (Gerson et al., 2005) in which

BOLD activation was observed during rapid discrimination of visual objects accompanied by a motor response.

====== **Figure 8 here** =======

Since MPA represents each IC equivalent dipole location by a Gaussian density and computes MPA domains in brain regions exhibiting significant local measure convergence, we may expect that equivalent dipoles positioned in or near MPA domains will have EEG measures similar to the domain exemplar measure. To verify this prediction, in Fig. 8A for one ERSP domain we plotted some such dipoles (e.g., those with total probability density within the domain above 0.05) and colored them by the correlation of their EEG measures with the domain exemplar. As expected, the majority of these dipoles have an ERSP similar to the domain exemplar. In Fig. 8B, domain exemplar ERSPs for Target and Nontarget conditions and their statistically masked difference (p<0.05) are plotted.

1.3.4 Simulation
To test and validate our MPA procedures, we conducted simulations to investigate the performance of the method across different noise levels and parameter choices.

====== **Figure 9 here** =======

We started by selecting four anatomical domains (Fig. 9A: R Superior Parietal Gyrus, L Inferior Occipital Gyrus, L Lateral Orbitofrontal Gyrus and R Superior Temporal Gyrus, from LONI LPBA40 atlas (Shattuck et al., 2008)) in MNI space as ground truth and assigned to each the ERSP pattern from one our RSVP-experiment domains. We then placed 31 dipoles by randomly selecting locations from the ground-truth domains and adding Gaussian spatial noise to the dipole locations using 12-mm std. dev. Gaussian noise to simulate localization error and subject variability in measured IC equivalent dipole positions. The number of dipoles per ground-truth domain (31) was selected to be the average number of dipoles for which more than 10% of their density, modeled by a truncated 3-D Gaussian, was located in an ERSP-measure domain of our RSVP experiment. We considered two simulation conditions: (1) assigning this ERSP patterns to simulated IC dipoles associated with each ground-truth domain (zero noise) (2) adding 0.2 dB RMS amplitude noise to the ERSP pattern associated with each IC dipole (simulating experiment noise).

We then sequentially added 142 other dipoles to the model, each placed at the brain volume location (in an 8-mm grid) farthest from all other existing dipoles. Pseudo-ERSP measures composed of random 0.2-dB white noise samples were assigned to these dipoles. The simulation thus contained the same number of brain dipoles as our RSVP experiment, with spatially coherent measure values only in the four model domains.

13

MPA was then performed on this simulated collection of dipole locations and associated ERSP measures. The resulting domains were then compared to ground-truth domains for the two simulation noise conditions mentioned above (Fig. 9B). We used two scoring methods to evaluate the performance of MPA method (a) Cohen's kappa (Cohen, 1960), a measure of inter-rater agreement (b) the average percentage of ground-truth domain locations that were associated with the correct domain in the results. In both scoring methods we accounted for permutations in domain labels and included the locations which should not be associated with any ground-truth domain as an extra category (they should not be assigned to any domains in the results).

====== **Table 2 here** ======

Table 2 shows MPA performance scores for simulation results with a voxel significance p-value threshold of 0.05, maximum exemplar correlation threshold of 0.8, and varying noise levels. To explore the sensitivity of MPA results to the choice of the location uncertainty parameter (the standard deviation of the Gaussian representing each dipole), we also tested different values of this parameter for two ERSP noise levels (noiseless and 0.2 dB). These simulation results show that MPA can recover brain domain locations with high accuracy ($> \%80$) in the presence of noise, and that using inaccurate dipole density extent priors (e.g., using a 10-mm or a 14-mm instead of the ground-truth 12-mm std. dev. for the spatial-perturbation Gaussian) has relatively little effect on their locations.

1.4 Discussion

The localized EEG source estimates returned by ICA decomposition bring closer the promise of performing near cm-scale functional cortical imaging using non-invasive EEG while retaining its fine temporal resolution. However, applying ICA-based EEG imaging to studies involving multiple subjects and/or sessions requires a method for combining IC source location and activity measure information for ICs decomposed from multiple data sets. Here we demonstrate a first application of measure projection analysis (MPA) to EEG data sets collected in a visual RVSP task and decomposed separately using extended infomax ICA. We compare the results of MPA to results of applying k-means clustering jointly to the same IC source locations and EEG measures. Results of MPA were consistent with IC clustering but depended on fewer parameters and provided statistical significance values. MPA applied to surrogate data derived from the RVSP data demonstrated that MPA results are not highly sensitive to prior parameter choices.

While here we feature application of MPA to group and condition statistics for standard event-related mean measures (ERPs and ERSPs), MPA may equally well be applied to any other continuous or event-related EEG measure, or indeed to any measure at all. For example, MPA applied to recovered IC equivalent dipole locations from an EEG session and a measure of the subject's memory ability might reveal differences in IC dipole density associated with better or

worse memory performance. Reliable differences in dipole density might arise from difference either in brain structure or dynamics during the EEG data collection. MPA has several other attractive features:

1.4.1 Relative Parsimony

Since across-subject and -session variability both in estimated and actual source locations and in dynamic EEG measure estimates are expected in any study, any model of subject group and/or session mean measures for a high-density EEG study must be probabilistic and therefore controlled by model expectations and statistical thresholds used in the analysis (in this, MPA applied to EEG data is similar to group-level analyses for fMRI data). Among such methods, the principle of parsimony (Occam's Razor) prefers methods that characterize the data variability (here, across data sets) using a minimal number of free parameters. Applying MPA to a single- or multi-dimensional EEG measure computed for a number of EEG sources, each tagged with an estimated source location in a standard anatomic head model, requires 1) a width parameter for the Gaussian density representing each source location, 2) a (p-value) significance threshold that can affect the size of the measure convergence subspace, and 3) a maximum domain exemplar measure similarity threshold used in domain clustering (the outlier detection threshold is an optional parameter). These MPA parameters are neurophysiologically interpretable and may not require sensitive tuning in applications to different studies.

In comparison, the PCA-based multi-measure source clustering approach introduced in (Makeig et al., 2002) and now available in EEGLAB (Delorme and Makeig, 2004) requires two parameters per dynamic EEG measure (the number of principal dimensions retained and the relative measure weighting value), plus a relative weight for equivalent dipole location and the number of clusters to create (e.g., four total independent parameters for one measure, six parameters for two measures, etc.). Since there is no statistically motivated method for choosing these parameters, they may in practice be set by the experimenter to produce most subjectively desirable results. Because of the relatively large number of such variables, and the sensitivity of final clustering results to their values, experimenter parameter settings may have profound effects on inferences at the group-level. This also introduces a significant and undesirable lack of objectivity in interpreting EEG data and hinders the calculating of significance statistics for group-level or session-level results. Even if well-justified methods were introduced to set the source clustering parameters, it would be still difficult to determine the statistical significance (including p-values) of cluster measure means because these statistical methods are often based on bootstrap null-hypothesis testing that is not easily and directly applicable to source clusters.

Recently an IC source clustering method called MAGMICK has been proposed by (Spadone et al., 2012). MAGMICK optimizes the relative weighting of different IC source measures so as to increase the mean silhouette value of IC clusters and selects the number of clusters found using modified K-Means clustering based on the constraint that two IC sources from the same session

should not be clustered together. Their results show that MAGMICK outperforms other direct IC source clustering methods applied to data from a sample MEG study.

However, the fact that session ICs are obtained by minimizing time-course independence over the whole experiment is not sufficient for the independence constraint conclusion made in MAGMICK. This is because ICA achieves maximal independence only for the whole time course of the experiment; ICs from the same decomposition may be transiently dependent, most likely in time periods in which EEG dynamics are non-stationary such as periods of significant ERP or ERSP activity. Lastly, MAGMICK does not provide statistical significance values for its clustering solution.

Thus, a strength of MPA is that it provides a relatively parsimonious method for data driven identification of brain regions exhibiting statistically consistent measure values.

1.4.2 Source Measure Consistency

MPA provides a statistical characterization of the subspace of brain source locations that exhibit significant EEG measure homogeneity, and identifies, among such locations, spatial domains with distinctive measure features. By contrast, neither PCA-based multiple-measure clustering (as formulated in EEGLAB) nor Group ICA approaches (discussed below) provide such statistics (i.e., tests to determine whether within each identified cluster or factor the computed source measures are significantly consistent with each other). For example, PCA-based clustering produced 15 clusters in our RSVP study, compared to only four MPA domains, but 9 of these clusters lacked significant measure homogeneity (measure convergence p-value, Eq. (A.3), at their centroid was higher than 0.05) and 8 of them did not have mean measures that were sufficiently distinct (correlation < 0.8) from other clusters.

1.4.3 Source Clustering Coherency

The MPA domain clustering procedure (used here to identify the four ERSP domains) is fundamentally different from the PCA-based clustering approach in that MPA, domain clustering is only employed to summarize projected results at significant brain locations and does not change the projected source measure values.

In contrast, cluster-mean values obtained by the PCA clustering method are highly dependent on the number of clusters and the specified relative measure weight parameters. Neither PCA-based source clustering nor Group ICA approaches use an explicit threshold for separating source clusters or factors based on measure differences. PCA clustering typically operates on a weighted combination of different measures, which prevents the use of meaningful similarity thresholds in threshold-based clustering (see Appendix B). In contrast, MPA uses meaningful similarity thresholds (for example, here a maximum measure correlation of 0.8) to identify separate brain-voxel domains whose nearby source measures have separable features.

Using different maximum correlation thresholds only changes the granularity of the segmentation of brain regions exhibiting significant measure consistency into domains, and does not fundamentally affect the values assigned to domains. For example, in the MP analysis shown here, changing the maximum domain measure correlation to 0.9 might identify more measure domains, though the exemplar measures of the added (sub)domains would be quite similar. In general this value must be set based on the expected degree of measure noise and variability in the data which influences how similar two domain exemplar measures could be before they should be considered practically the same. Alternative clustering methods developed for identifying regions of similarly activated voxels in fMRI data, such as Cluster-Based Analysis (CBA) (Heller et al., 2006), might also be applied to MPA. The Affinity clustering approach used in the MPA toolbox (Appendix B) has the advantage of finding the appropriate number of clusters based on the given similarity threshold without having to specify a final number of clusters beforehand,

1.4.4 Cluster membership
PCA-based IC source clustering limits the types of group-level analysis methods that may be applied to EEG data. For example common clustering methods (e.g., k-means or linkage clustering) output a set of binary ("hard decision") cluster membership values: each source either fully belongs to a certain cluster or not. As the formation of these clusters is often highly dependent on the multitude of clustering parameters, it is difficult to separate the effect on the clustering results due to choosing these parameters from the contributions of group-level differences in source features.

As an example, a cluster of interest (e.g., having a particular target ERP feature) may mostly contain sources associated with a certain participant subgroup. At the same time, sources with similar features may exist in nearby clusters and may have been included if a lower number of clusters or slightly different weight parameters were applied to source measures during clustering. It then becomes unclear whether participants have meaningfully different measures (either in terms of source locations or ERP measure features) from a parent or alternate population, or whether the aggregation of sources from this subject group into a particular cluster is an artifact of selecting a particular set of clustering parameters. This problem could be alleviated if sources were given fractional (fuzzy) memberships and if noise were not introduced during the quantization of membership values by the clustering procedure. MPA allows such improvements by adopting a probabilistic spatial representation of source locations.

1.4.5 Cluster shape
MPA operates in brain source domain coordinates and thus gives source domains that are not restricted in shape and may even be discontinuous. For example, a single domain representing bilaterally symmetric source activations may account for synchronous activity within two non-

contiguous (but perhaps highly connected) cortical areas. PCA-based IC clustering, on the other hand, does not explicitly specify brain areas whose EEG-source signals are reactive within a class of experimental conditions. K-means clustering, in particular, is biased towards creating spherical clusters. Further, when an IC cluster is represented by the spatial centroid of its member IC equivalent dipole locations, the spatial extent of each cluster is not investigated statistically. Here MPA provides a statistically supported, data-driven model of cortical regions that exhibit consistent measure features, and the regions so identified may be readily compared to results of other functional imaging experiments, for example reported results of fMRI studies.

1.4.6 Cluster equivalence across measures

Here we propose that MPA should be applied to only one dynamic measure at a time. Another problem associated with PCA-based IC clustering stems from the fundamental assumption of IC cluster equivalence across all EEG measures. In this method it is assumed that those ICs that are similar in one respect (for example, in ERP time courses) are also similar in other aspects (say in their ERSPs or mean spectra), so that combining different measures before clustering (e.g. by concatenating them to form the IC pre-clustering array, Fig. 2B) should produce better results (cluster distinctiveness is increased by combining measures). This rests on the assumption that the similarity structures of each measure of interest are dominated by an identical or at least compatible IC cluster structure. If this assumption is violated, as our results in Fig 3 indicate for the RSVP data, combining different IC measures may actually degrade clustering results since they attempt to merge conflicting IC similarity structures.

For example, imagine a situation in which certain brain areas produce an ERP response to a stimulus event class (e.g., visual targets), but that significantly different, yet overlapping, brain areas produce transient mean (ERSP) changes in the IC power spectrum following events of this class. An IC clustering performed on a combination of these two measures (plus equivalent dipole locations*) will at best find the spatial overlap between the two areas associated with ERP and ERSP measures, potentially a much smaller area than the areas associated with each EEG measure separately. If the goal of the analysis is, for example, to learn about ERP responses to visual targets, it would appear better to use only the ERP measures and equivalent dipole locations instead of including both ERP and ERSP measures, as we propose for MPA.

It may also be possible to subdivide multi-dimensional measures into sub-regions (for example, ERP latency ranges or time/frequency regions) and apply MPA to each measure region, a possibility that may deserve further examination.

1.4.7 Subject comparisons

When IC process clustering gives disjoint IC clusters, it is not always easy to compare the EEG dynamics of each subject to the group cluster solution. Some clusters may contain no ICs belonging to some subjects. Since so many variable parameters enter into a particular clustering

solution, it may be difficult to argue that the absence of a cluster IC from a given subject necessarily reflects the absence of equivalent EEG source activity for that subject. This issue worsens as the number of clusters increases and fewer subjects contribute ICs to each cluster. MPA overcomes this difficulty by probabilistic representation of dipole locations and abandoning the notion of discrete, disjoint IC clusters.

1.4.8 Group-Level ICA decomposition

ICA was initially applied at the group level as spatial ICA decomposition of group fMRI data (Calhoun et al., 2001), (Schmithorst and Holland, 2004), (Beckmann and Smith, 2005) (Esposito et al., 2005). This method has also been applied to resting-state EEG (Congedo et al., 2010) and to joint decomposition of concurrently recorded EEG-fMRI data (Moosmann et al., 2008), (Eichele et al., 2009), (Kovacevic and McIntosh, 2007), (Calhoun et al., 2009). Group-ICA is implemented in the EEGIFT toolbox (http://icatb.sourceforge.net/) for EEG analysis. In this approach, data sets from multiple subjects are either, (a) concatenated in time, assuming common group IC scalp topographies, or (b) concatenated as separate channels, after some preprocessing (e.g., PCA-based dimensionality reduction), assuming shared event-locked group IC component measure features.

Each of these methods violates the physiological assumptions underlying ICA, arising from differences in brain anatomy and volume conduction (Nunez and Srinivasan, 2006). Concatenating EEG recordings from different subjects along the time/latency dimension, and implicitly assuming that subject ICs share scalp maps, ignores significant differences across subjects in cortical anatomy, in particular differences in scalp projection topography arising from differences in cortical folding, and in functional specificity of corresponding cortical areas (Onton and Makeig, 2006). Concatenating event-related response time series data from different subjects in the spatial (channel or PCA-reduced channel) dimension, on the other hand, assumes that ICs share strong feature similarities, in particular event-related response time courses. Thus, for example, for all but the very earliest (brainstem and primary cortical) ERP features a highly unrealistic degree of common event-related time-locking is assumed. Also, this ERP-oriented procedure is intrinsically unable to capture time-locked but not phase-locked dynamics, (as, e.g., captured by ERSPs).

In addition, during group-ICA preprocessing (as described in (Rachakonda et al., 2011)), the channel data are usually strongly reduced in dimension using PCA (e.g., from 64 channels to 30 principal components) to keep the final number of dimensions after concatenation (across subjects) manageable for application of ICA. As the number of participants increases, even more aggressive PCA dimensionality reduction is necessary to keep the dimensionality of the concatenated data more or less constant (since the number of time points used in group-ICA remains constant and the final ICA requires a certain number of time-points for calculation of each weight in the unmixing matrix). But since PCA only takes into account second-order

(correlation) dependencies across channel data, it has lower performance in terms of reducing mutual information compared to ICA, and therefore the remaining dimensions after PCA preprocessing may potentially lack subspace information necessary for proper ICA separation at either the single subject or group levels.

Another issue with applying group ICA decomposition to event-related EEG data concatenated across channels is that it injects a bias towards finding patterns that are common across subjects. PCA-reduced activities from each subject are (to some degree) time-locked to the event, and subsequent group ICA processing tries to find components that are common across subjects. ERPs for a subset of these group ICs may then just be an artifact of the Group ICA decomposition process (since the common subspace across subjects is amplified and concentrated into a few Group ICs). This bias in data preparation makes calculating proper statistics difficult if not impossible. One would need to perform some type of bootstrap permutation test to estimate the significance of the common activity discovered by this approach, though performing a large number of Group-ICA decompositions on surrogate trial collections may prove computationally impractical.

There are two newer methods that improve on group-ICA for performing group-level joint decomposition: Multiset Canonical Correlation Analysis (M-CCA) (Li et al., 2009), which uses an extension of Canonical Correlation analysis to maximize the correlation among the extracted source activations, and blind source separation by joint diagonalization of cumulant matrices (Li et al., 2011) (Via et al., 2011). These algorithms avoid the PCA dimensionality reduction of group-ICA but they both also assume that significant linear correlations are present across source activations. EEG source activities across a group of subjects can only be hypothesized to be similar or linearly correlated if they are all time-locked to a relevant event type (e.g., a rhythmic stimulus) and their duration are limited to data intervals that contain significant ERP features, often less than a second after (or in some cases before) the event. Outside of such time periods, no reliable correlation should exist that can be exploited by group-level decomposition methods. This limits the applicability of these methods for high-density EEG since the portion of data that can be assumed to contain group-level correlations is much shorter than the whole recording so there will be less data available to perform blind source separation (e.g., as compared to Infomax ICA decomposition of data from the entire session). This is likely to adversely affect the performance of the decomposition.

Also, many EEG phenomena occur in time-frequency domain in such a way as to contribute few or no features to average ERPs. In particular event-related spectral perturbations (ERSPs) such as those induced by changes in alertness level (Makeig and Jung, 1995) measure event-related changes in spectral source power regardless of the level of event-locked phase coherence that produces the event-locked ERP. Since all group-level decomposition methods discussed above operate in the time domain, they are not amenable to time-domain Group ICA approaches.

Recently, (Hyvarinen, 2011) has suggested a method to test the inter-subject consistency of ICA solutions statistically based on scalp-map similarities. Because of the differences in dipole orientation arising from between-subject variations in cortical volumes and folding, ICs represented by dipoles in the same functional brain area may have significantly different scalp maps. Hence this method is more suitable for different sessions of the same subject and should only provide a lower bound on inter-subject consistency (since similar scalp maps are typically associated with similar ICs but not necessarily *vice versa*). The same argument also applies to IC clusters obtained from this method, as they do not take into account equivalent dipole locations associated with ICs.

1.5 Conclusion

Here we have introduced measure projection analysis (MPA), a statistical method for combining source-localized EEG measure information across data sets. We also have presented empirical and simulated results and have discussed the advantages of measure projection relative to previously proposed independent component clustering methods. Measure projection puts results of EEG research into the same brain imaging framework and coordinate system as other brain imaging methods, thereby allowing EEG to be treated and used as a three-dimensional functional imaging modality.

1.6 ACKNOWLEDGMENTS

Appendix A

Measure Projection Analysis (MPA) Method Description

Measure Projection Analysis (MPA)

Problem. A subset of EEG independent component (IC) processes obtained by applying ICA decomposition to preprocessed channel activities from each recording session of a study consisting of multiple sessions and/or subjects may be accurately modeled by single (or in some cases bilaterally symmetrically located pairs of) equivalent dipoles located in the co-registered standard MNI brain coordinate system (Delorme et al., 2012). In this analysis we only consider equivalent dipoles within the MNI model brain volume (*V*), although the proposed method should also be separately applicable to equivalent dipoles located outside brain, such as in the eyes and at attachments of neck muscles to the scalp. Furthermore, we do not consider ICs that cannot be modeled using a single (or in some cases as dual symmetric) equivalent dipole model.

In practice, in any decomposition there may be an IC that can be accurately modeled by an equivalent dipole $D(x)$ located at any model brain location $x \in V \subset R^3$. Consider a measure vector $M(x)$, obtained by vectorizing ERP time-course or ERSP time-frequency image, associated with an IC with an equivalent dipole $D(x)$. Measure vectors typically estimate mean event-related changes in IC source activity, which are often monotonically related to the recorded scalp potential changes accounted for by the IC. Because of subject differences in skull thickness and brain dynamics, these measure vectors may have dissimilar and unknown differences in scale and/or offset across subjects. For example, two subjects may show a similar (circa 10-Hz) central-lateral mu rhythm desynchronization pattern (reduction in power) during hand-motor imagery, but the maximum dB change for each subject may be quite different, as reflected in ERSP measures for one or more ICs from each subject's data.

During the set of experimental sessions in the study, up to *n* IC processes associated with *n* distinct equivalent dipoles $D_i \equiv D(x_i)$ (with indices $x_i, i = 1, .., n$) may be active. We desire to estimate an interpolated measure vector $M(y)$, defined across possible brain locations $y \in V$, and to estimate the statistical significance (p-value) of this assignment at each of these locations. These p-values are associated with the (null) hypothesis that the measure vectors have a random spatial distribution in the brain and there is no significant similarity between them within neighborhoods centered at brain locations $y \in V$.

Approach. Let σ be the standard deviation of a spherical 3-D multivariate Gaussian with covariance $\sigma^2 \cdot I$ centered at an estimated dipole location $\hat{x}_j$. We spherically truncate the density at a radial distance (to center) of $t\sigma$. After normalization to insure that densities both deep inside the brain volume and near the brain surface have unity mass within the brain volume, this

truncated Gaussian is used to represent the probability density of the true equivalent dipole location given its estimated location. The parameter σ encapsulates errors in dipole localization arising through errors in tissue conductivity estimates, head co-registration, numerical data decomposition, data noise, and between-subject variability in the locations (with respect to the head model) of equivalent functional cortical areas. We place a renormalized truncated Gaussian at each estimated dipole location. According to this model, the probability of estimated dipole D_j being truly located at position $y \in V$ is $P_j(y) = TN(y; \hat{x}_j, \sigma^2 \cdot I, t)$, where $\hat{x}_j$ is the estimated location of D_j (and TN is a normalized truncated Gaussian distribution). For an arbitrary location $y \in V$, the expected, or *projected*, value for the measure vector is

$$E\{M(y)\} = \langle M(y) \rangle = \frac{\sum_{i=1}^{n} P_i(y) M_i}{\sum_{i=1}^{n} P_i(y)} \tag{A.1}$$

If an equivalent dipole were truly located at $y \in V$, it would have the measure projection $M(y)$ provided by (A.1). We want an estimate of $M(y)$ given by $\langle M(y) \rangle = \sum_{i=1}^{n} \bar{P}(y) M_i$, where $\bar{P}(y)$ is the probability that $M_i(y) = M(y)$. Since the probabilities have to sum to one ($\sum_{i=1}^{n} \bar{P}_i = 1$), it is natural to define $\bar{P}_i(y) \equiv \frac{P_i(y)}{\sum_{i=1}^{n} P_i(y)}$. This gives (1) and shows that our estimate is given by a convex combination (weighted average) of measure values M_i that depends on equivalent dipole location $y \in V$.

Now that we have an estimate of the measure vector at each brain voxel location, we need to estimate the probability distribution of projected measures $M(y)$ under the null hypothesis that an estimated measure vector is actually produced by a random, set of measure vectors M_i in the spatial neighborhood. This is necessary to be able to assign any statistical meaning to the projected values. There are at least two ways to do so.

The first is to calculate p-values for each dimension of projected measure vector $M(y)$. There are, however, two drawbacks to this approach. Firstly, unknown scale and constant offset differences associated with measure values for different subjects may act as additional sources of variability (unless an effective measure normalization method is applied) reducing the power of statistical testing. Second, if measure vector $M(y)$ is high-dimensional, the issue of robustly correcting for multiple comparisons becomes critical, especially when a high-resolution spatial grid is placed in the brain volume. For example, an ERSP measure may typically consist of a

matrix of 200 latencies by 100 frequencies giving 20,000 dimensions -- if brain voxels with 8-mm spacing are investigated, there will be about 4,000 locations examined, each associated with a 20,000-dimension vector. This would result in performing about 8×10^7 t-tests or some other type of null-hypothesis tests, which is undesirable: although methods for robust correction for multiple comparisons, including cluster-based techniques (Maris and Oostenveld, 2007) and Gaussian random field theory (Worsley et al., 2004) have been developed for high-dimensional data such as time-frequency images and fMRI voxel maps, use of these methods require assumptions such as joint Gaussianity or smoothness. Thus, further investigation is needed to determine the applicability of these methods to MPA.

Measure convergence. An alternative method for obtaining significance values is to identify brain areas or *neighborhoods* that exhibit statistically significant similarities in one or more measures between IC equivalent dipoles within the neighborhood. To do so, we define the quantity $C(y)$ (measure convergence) at each brain location $y \in V$

$$C(y) = E\{S(y)\} = \frac{\sum_{i=1}^{n} \sum_{j=1, j \neq i}^{n} P_i(y) P_j(y) S_{i,j}}{\sum_{i=1}^{n} \sum_{j=1, j \neq i}^{n} P_i(y) P_j(y)} \tag{A.2}$$

In this equation, $P_i(y)$ is the probability of dipole i being at location $y \in V$ and $S_{i,j}$ is the degree of similarity between measure vectors associated with dipoles i and j. Convergence $C(y)$ is the expected value of measure similarity at location $y \in V$ assuming that the joint probability of each dipole pair i and j being located at $y \in V$ can be factorized as $P_i(y) P_j(y)$ (based on the independence assumption). Problems caused by unknown scaling and offsets may be avoided by choosing a similarity matrix impervious to these distortions, such as normalized mutual information or linear correlation.

Calculated convergence $C(y)$ is a scalar and is larger for areas in which the measures associated with local ICs are homogeneous (similar). The probability of making an error of Type I may be obtained for each brain location by comparing $C(y)$ to a distribution of surrogate convergence values $C'(y), i = 1, ..., k$ constructed from k randomized surrogates. Each surrogate convergence value is obtained by destroying the association between dipoles and their measure vectors by randomly selecting, with substitution, n surrogate measure vectors $M'_i, i = 1, ..., n$ and associating them with dipoles $D_i, i = 1, ..., n$. The surrogate similarity matrix $S'_{i,j}$ is obtained by calculating similarities between these surrogate measure vectors.

By repeating the process above k times, a distribution of surrogate convergence values $C_i'(y), i = 1,.., k$ at each brain location $y \in V$ is obtained and the significance of convergence $C(y)$ is obtained by comparing it to the right tail of this null distribution. This p-value is equal to the proportion of surrogate $C(y)$ values higher than the actual convergence value $C(y)$

$$p - value\{C(y)\} = \frac{\#\{i : C'_i(y) > C(y); i \in 1,.., k\}}{k} \tag{A.3}$$

After p-values are calculated for each brain voxel, they may be corrected for multiple comparisons across MNI brain grid locations and only those voxels with significant measure convergence (e.g., $p < 0.05$ after correction for multiple comparisons) selected for further analysis. Since $C(y)$ is a scalar value and often has a much lower dimension than measure value $M(y)$, the multiple comparison problem is more manageable when dealing with convergence values.

Spatial domain clustering. Projected measure vectors associated with these locations may then be clustered to identify spatial *domains* exhibiting similar measure vectors in the data. Note that spatial domain clustering in MPA is different from IC clustering: in MPA, clustering is performed on the projected measure vectors $M(y), y \in V$ at each brain space voxel, so changes in domain clustering parameters do not change the voxel measures themselves. MPA operations such as subject or condition comparisons can act directly on these voxel measures and do not solely depend on domain exemplars. Mean measures of IC clusters, on the other hand, may take different values depending on the IC clustering parameters used, and only these mean measures are used in subject or group comparisons.

MPA toolbox. We have implemented the MPA method under MATLAB (The Mathworks, Inc.) as a plug-in for EEGLAB (Delorme and Makeig, 2004). The Measure Projection Toolbox (MPT), freely available for download at http://sccn.ucsd.edu/wiki/MPT, includes high-level MATLAB software objects and methods that simplify the application of MPA to EEG studies. The toolbox also utilizes the probabilistic atlas of human cortical structures LPBA40, provided by the LONI project2 (Shattuck et al., 2008), to define anatomical regions of interest (ROIs) and find ratios of domain dipole masses for cortical structures of interest.

---

[2] Available for download at http://www.loni.ucla.edu/Atlases/Atlas_Detail.jsp?atlas_id=12

Appendix B

Threshold-based Clustering and Outlier Rejection using Affinity Propagation

Estimating the optimum number of clusters is an outstanding problem in the field of data clustering (Milligan & Cooper 1985, Gordon 1996). There have been several solutions proposed for this problem, each based on certain assumptions regarding noise and underlying cluster structure (Hardy 1996, Kryszczuk & Hurley 2010). On the other hand, in practice often the goodness of a clustering solution is evaluated by comparing a subset of its properties (e.g., the dissimilarity between cluster centers) with common domain or expert knowledge. For example, suppose that linear correlation is used as a similarity measure to obtain clusters using agglomerative hierarchical clustering (Hastie et al. 2009) and the clustering solution contains twenty clusters, two of which have exemplars (data points comprising cluster centers) more similar to each other than 0.95. Then additional domain knowledge such as assumed or expected noise level may allow us to infer that a better solution could be obtained with fewer clusters.

Another issue that arises in many practical clustering applications is the existence of outliers and their effect on the clustering solution. Outliers are defined as data points that are far from all cluster exemplars (centers) and should therefore not be assigned to any of them (in which case they can be grouped into a special 'outlier cluster'). A common way to deal with this issue is to obtain a clustering solution while treating outliers as any other data point, and then removing them *post hoc* in some principled manner. For example, a simple way to do this would be to remove all points that are further than a given distance threshold to any cluster center (such a method would be especially applicable if a distance or similarity threshold could be established based on domain or expert knowledge). A problem with this approach is that the clustering solution is affected by all data points, in particular the outliers which are removed in the second step. In cases in which the outliers in the total data set are significant in number, or are much more distant than regular points from cluster centers, the clustering solution may be visibly deteriorated by their presence.

Here we propose the use of Affinity Propagation clustering (Frey & Dueck, 2007) to address the abovementioned difficulties by incorporating two threshold values based on domain knowledge. Affinity propagation method finds exemplars by passing real-values messages between pairs of data points. The magnitude of these messages is based on the affinity of each point for choosing the other as its exemplar. This algorithm is shown to be equal or better than K-means in minimizing clustering error on large datasets. It also only requires a pair-wise similarity matrix as input, a property exploited by our proposed method to find an appropriate number of clusters while ignoring outliers during the clustering process. Although our method is based on the use of Affinity Propagation clustering, it may, in principle, be combined with any clustering method that accepts a pairwise similarity matrix.

Let $S_{n \times n}$ be a pairwise similarity matrix for n input points $P_i, i = 1, \cdots, n$ to be clustered. Our objective is to find a clustering solution in which:

(a) Outliers, defined by points that are less similar than $T_o \in R$ to any cluster exemplar (centroid) E_k, are assigned to a special outlier cluster.
(b) The data are clustered into the maximum number of clusters such that no cluster exemplar E_k is more similar to another than a given similarity threshold $T_e \in R$.

To achieve objective (a), we augment the original pairwise similarity matrix $S_{n \times n}$ to include a new *virtual point* P_{n+1} that has a constant similarity T_o to all original data points P_i:

$$S'_{n+1,n+1} = \left[\begin{array}{ccc|c} S_{1,1} & \cdots & S_{1,n} & T_0 \\ \vdots & & \vdots & T_0 \\ S_{n,1} & \cdots & S_{n,n} & T_0 \\ \hline T_0 & T_0 & T_0 & T_0 \end{array} \right]$$

(B.1)

The augmented similarity matrix $S'_{n+1,n+1}$ is then used for clustering.

During the clustering process, points compete for becoming exemplars of others. These dynamically formed exemplars compete for assignment to data points and since the virtual point P_{n+1} has a constant similarity T_o to all other points, any point which is less similar than T_o to all exemplars will be assigned to the cluster which contains the virtual point as its exemplar. This point hence becomes an exemplar for all outlier points in the data.

After the clustering process is finished, one of the following conditions will be met:

1. There are one or more outliers in the data, in which case they will be assigned to a cluster that includes the virtual point (see Fig. B.1C).
2. There are no outliers in the data and the virtual point is assigned as the exemplar of a cluster with only one member (itself).
3. There are no outliers in the data, but the virtual point is assigned to a cluster that is not an outlier cluster.

To distinguish between conditions 1 and 3 above, we can calculate the similarity between all exemplars and members of the cluster that includes the virtual point. If any similarity value is greater than T_o then condition 3 must be the case. Our use of an augmented similarity matrix thus achieves the first goal of separating outlier points during the clustering process.

To achieve objective (b) we begin by clustering $S'_{n+1,n+1}$ into a minimum number of clusters (1 or 2) and iteratively increase the number of clusters (if using Affinity Propagation, this is achieved by increasing the similarity value assigned between each data point and itself in the similarity matrix, which indirectly controls the number of clusters). In each iteration we calculate the minimum similarity $T_{\min}$ between cluster exemplars and compare it with T_e. If $T_{\min} > T_e$ then the procedure terminates and returns the clustering solution obtained in the previous iteration, satisfying objective (b).

====== **Figure B.1 here** ======

Fig. B.1A shows a simulated 2-D point cloud generated by adding to a low uniform point distribution two rectangular areas of increased probability density. Fig. B.1B shows Affinity Propagation clustering results using maximum exemplar similarity $T_e = 0.2$ and no outlier detection. Of the four clusters produced by this solution, two consist mostly of outlier points. Fig. B.1C shows the clustering solution obtained using outlier detection with $T_o = 0.2$ and $T_e = 0.2$. Here, the two high-density areas are separated into distinct clusters and other points are assigned to a third 'background' cluster.

Table 1

| ERSP Domain	Nearby Clusters	Anatomical Area(s)	Brodmann Area(s)
1	11, 14	(Dominated by eye-artifact ICs)	**N/A**
2	12, 15	R Middle Occipital Gyrus (0.36) L Middle Occipital Gyrus (0.26) R Inferior Occipital Gyrus (0.09) L Inferior Occipital Gyrus (0.08) R Superior Occipital Gyrus (0.05) R Lingual Gyrus (0.04) R Inferior Temporal Gyrus (0.03) R Angular Gyrus (0.02) R Middle Temporal Gyrus (0.02)	**BA 18 (0.34) Secondary visual (V2)** **BA 19 (0.34) Associative visual (V3)** BA 37 (0.11) BA 39 (0.06) BA 17 (0.06), Primary visual (V1)
3	1	L Superior Occipital Gyrus (0.19) L Cuneus (0.16) L Middle Occipital Gyrus (0.15) R Cuneus (0.12) R Superior Occipital Gyrus (0.10) L Superior Parietal Gyrus (0.06) L Lingual Gyrus (0.04) L Precuneus (0.03) L Superior Temporal Gyrus (0.02) R Middle Occipital Gyrus (0.02) R Superior Temporal Gyrus (0.02) R Lingual Gyrus (0.02)	**BA 18 (0.33) Secondary visual (V2)** BA 19 (0.15) Associative visual (V3) BA 31 (0.13) BA 17 (0.12) Primary visual (V1) BA 7 (0.06) Somatosensory Association
4	4	L Superior Parietal Gyrus (0.27) L Postcentral Gyrus (0.27) L Supramarginal Gyrus (0.22) L Angular Gyrus (0.12) L Precentral Gyrus (0.10)	**BA 40 (0.37) Spatial / Semantic Processing** BA 7 (0.12) Somatosensory Association BA 3 (0.11) Primary Somatosensory BA 2 (0.10) Primary Somatosensory BA 4 (0.09) Primary Motor BA 39 (0.06)

Table 2

| Mean MPA Performance Score (std)	Cohen's kappa Ratio (kappa, max possible)	Domain Dipole Noise Amplitude	Mean Domain Dipole SNR (std)	Extra Dipole Noise Amplitude	Projected Gaussian std. deviation (mm)
0.82 (0.21)	0.82 (0.63, 0.78)	0	1	0.2	12
0.85 (0.20)	0.84 (0.62, 0.73)	0	1	0.2	14
0.81 (0.19)	0.78 (0.63, 0.8)	0	1	0.2	10
0.93 (0.11)	0.9 (0.5, 0.56)	0.2	0.88 (0.09)	0.2	12
0.93 (0.10)	0.93 (0.47, 0.51)	0.2	0.88 (0.09)	0.2	14
0.89 (0.16)	0.84 (0.51, 0.61)	0.2	0.88 (0.09)	0.2	10
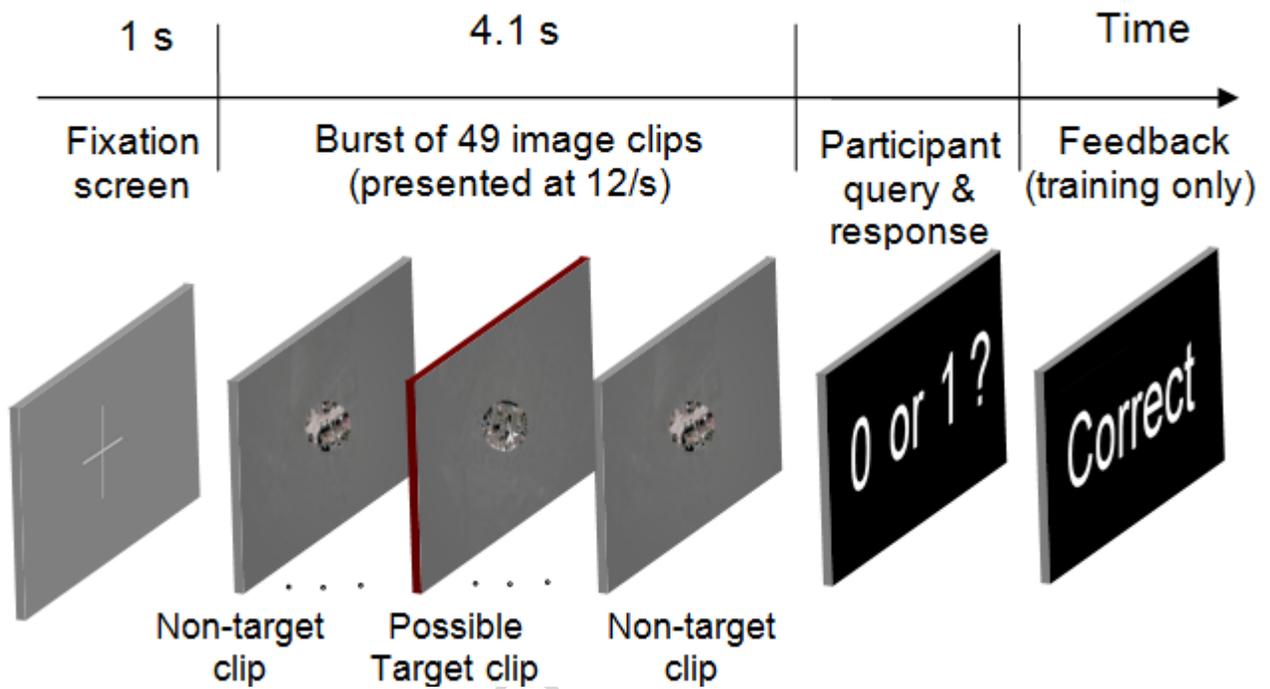
Fig. 1. Timeline of each RSVP burst. Participant response feedback ('Correct' or 'Incorrect') was delivered only during Training sessions (rightmost panel).
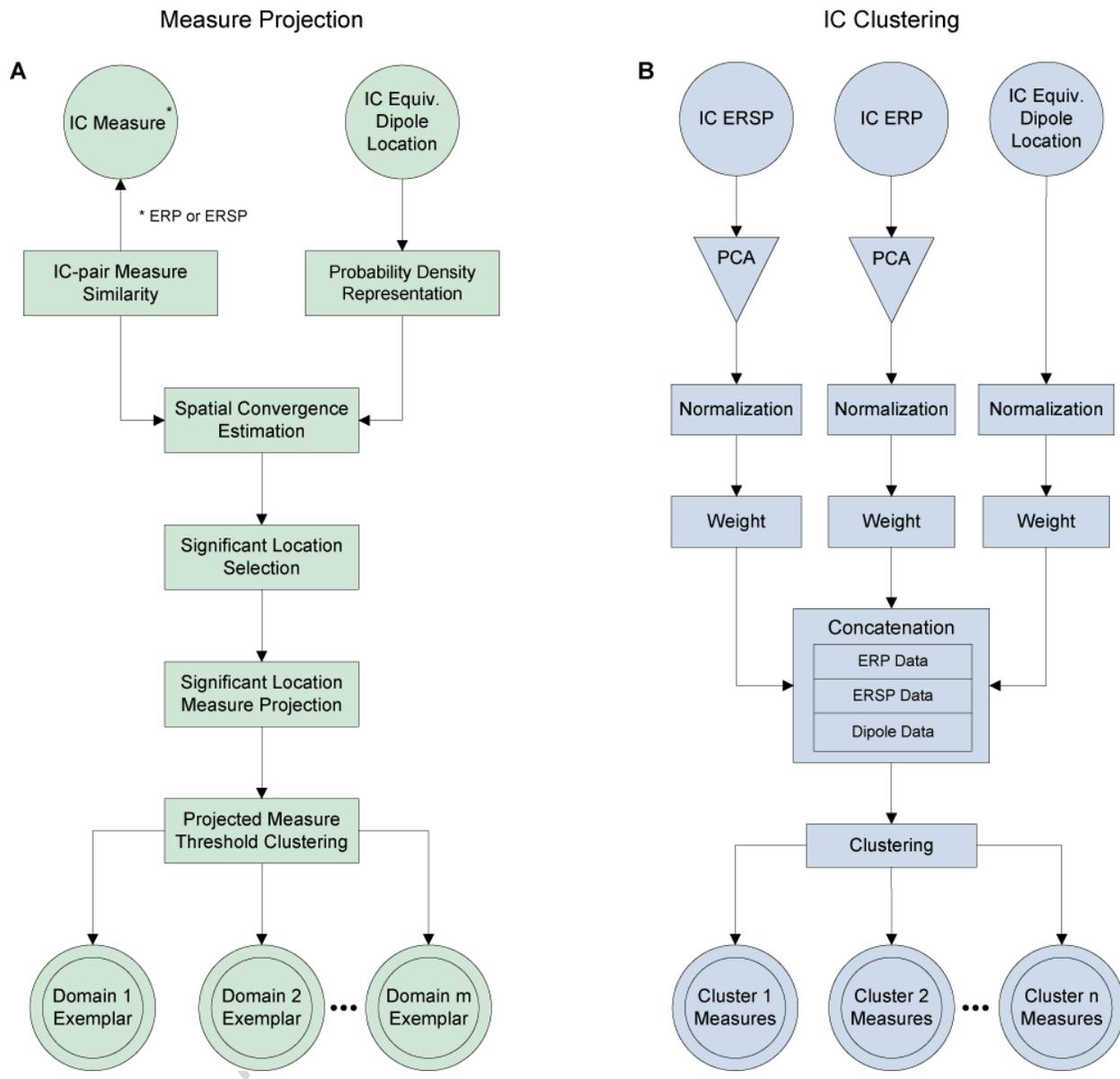
Fig. 2. Finding equivalent IC processes across subjects and/or sessions: **(A)** Steps performed during measure projection analysis (MPA) to identify brain voxel domains associated with significantly different measures of independent component (IC) processes whose brain source locations are each tagged by the location of the IC equivalent dipole. **(B)** Steps performed during PCA-based clustering to find IC process clusters each composed of ICs with nearby equivalent dipole locations and similar measures. Whereas PCA-based clustering solutions may *simultaneously consider* multiple non-dipole EEG measures (for example, condition-mean ERPs and ERSPs), in MPA finding spatial domains supporting each condition-mean measure is performed *separately*.
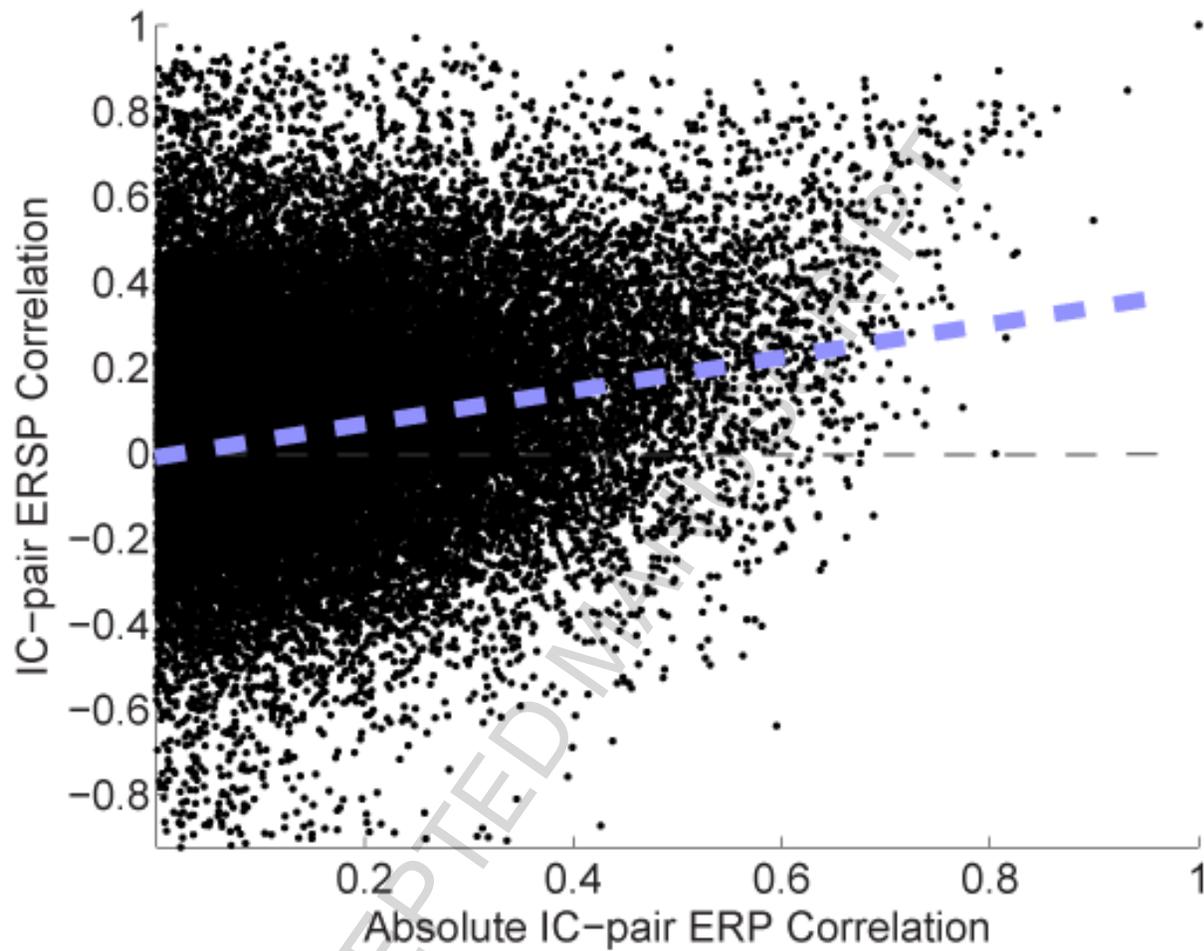
Fig. 3. IC-pair ERP and ERSP similarities. Absolute-value ERP similarities are used to overcome the inherent ambiguity of the polarity of IC activations. Dashed line displays the best least-squares linear fit (Pearson correlation coefficient = 0.26).
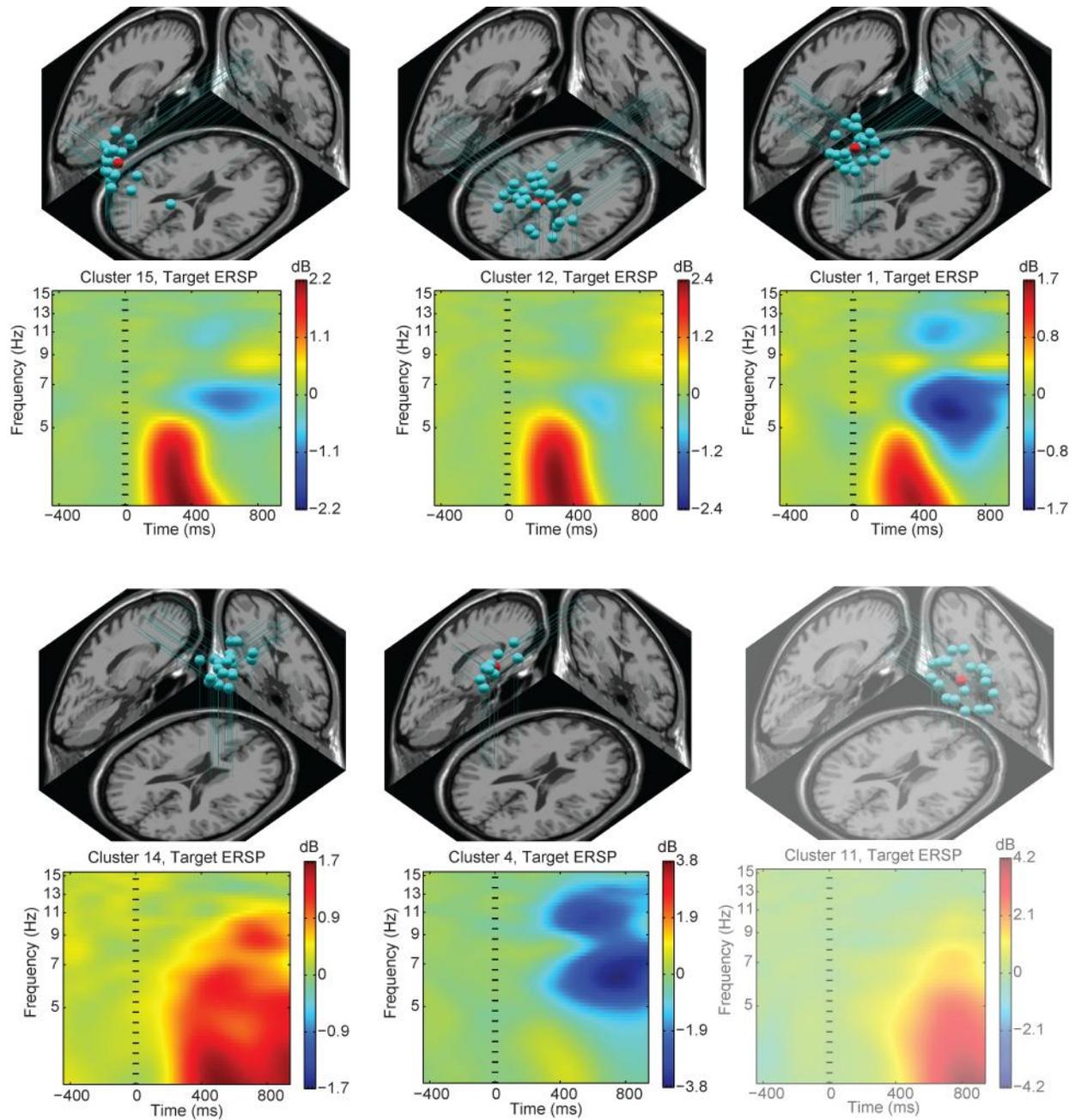
Fig. 4. Dipole locations and cluster-mean ERSPs for 6 of 15 IC clusters obtained from PCA-based clustering (see Fig. 2B) having relatively large Target event-related ERSP values, most in the low theta frequency band (each ERSP maxima equal or exceeding 1.7 dB). Cluster 11 is dominated by components accounting for eye movement artifacts.
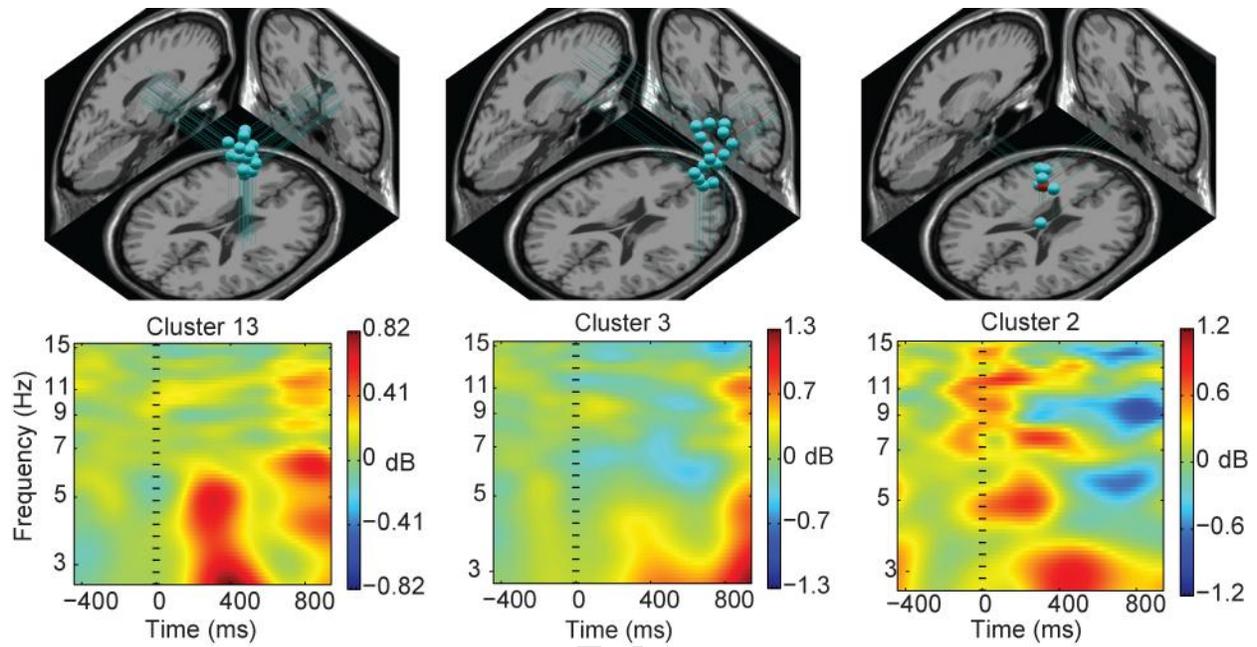
Fig. 5. Dipole locations and mean Target ERSPs for a subset of clusters with weak ERSP values (each with absolute maxima lower than 1.3 dB; compare Fig. 4).
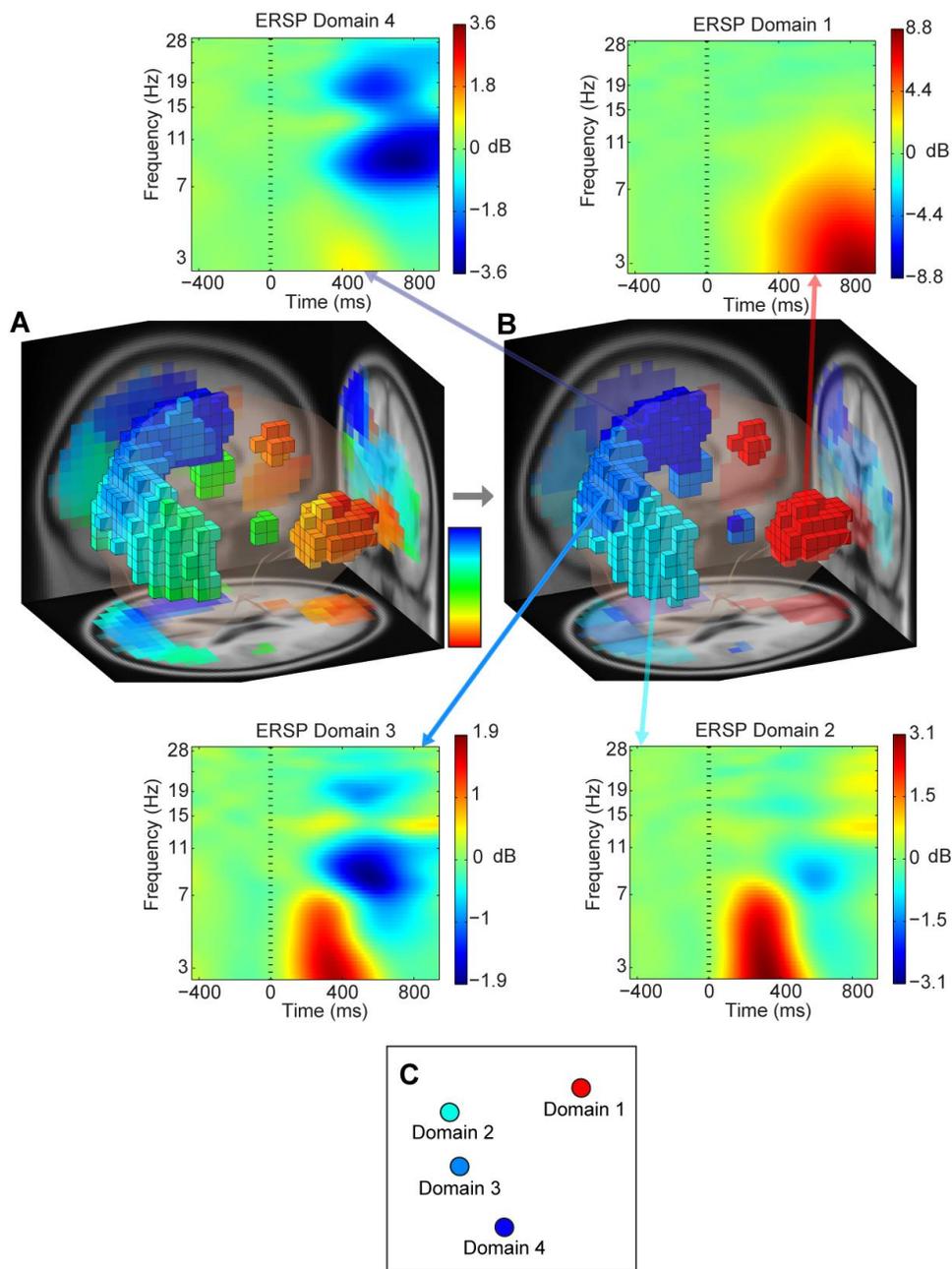
Fig. 6. Measure Projection Analysis (MPA) of ERSP (see Fig. 2A): **(A)** Voxels representing locations with significant convergence (p < 0.075) colored by multi-dimensional scaling (MDS) mapping of projected Target ERSP measures to hue (MATLAB 'hue' colormap values in the 0-0.69 interval, from red to blue). **(B)** Four domains identified in the projected measure values, colored by 1-D MDS of the projected measure at their exemplar voxel. **(C)** 2-D MDS image of exemplar similarities of the four domains. Note that Domain 1 (red, eye activities) is relatively distant from the other three Domains (blue, posterior cortex).

36
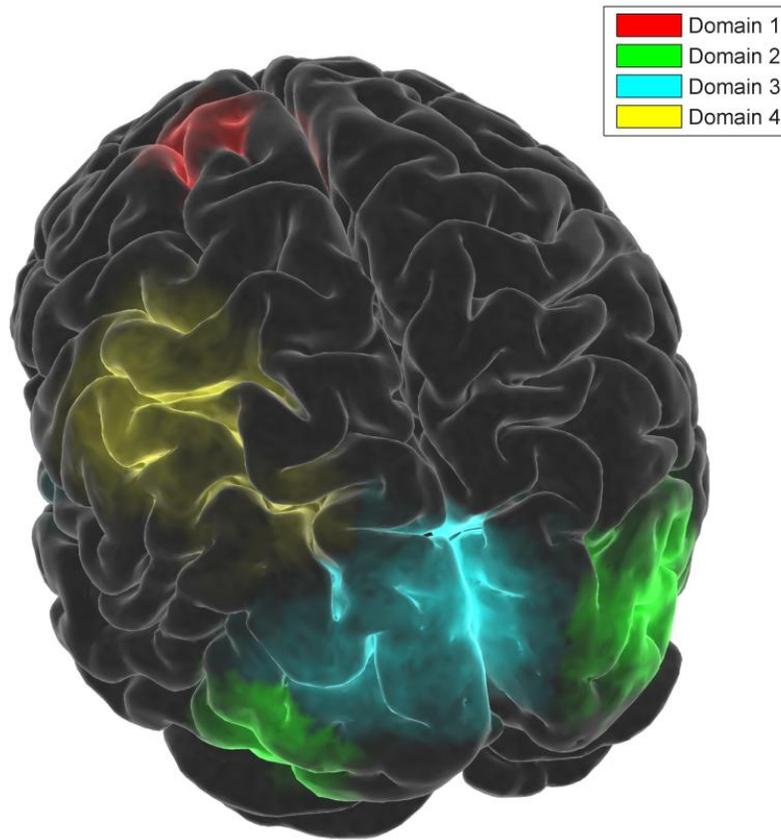
Fig. 7. Alternative visualization of ERSP domains projected onto the template MNI cortical surface. Each cortical surface voxel is illuminated based on the domain color and total dipole density from brain-grid voxels located radially below the surface polygon.
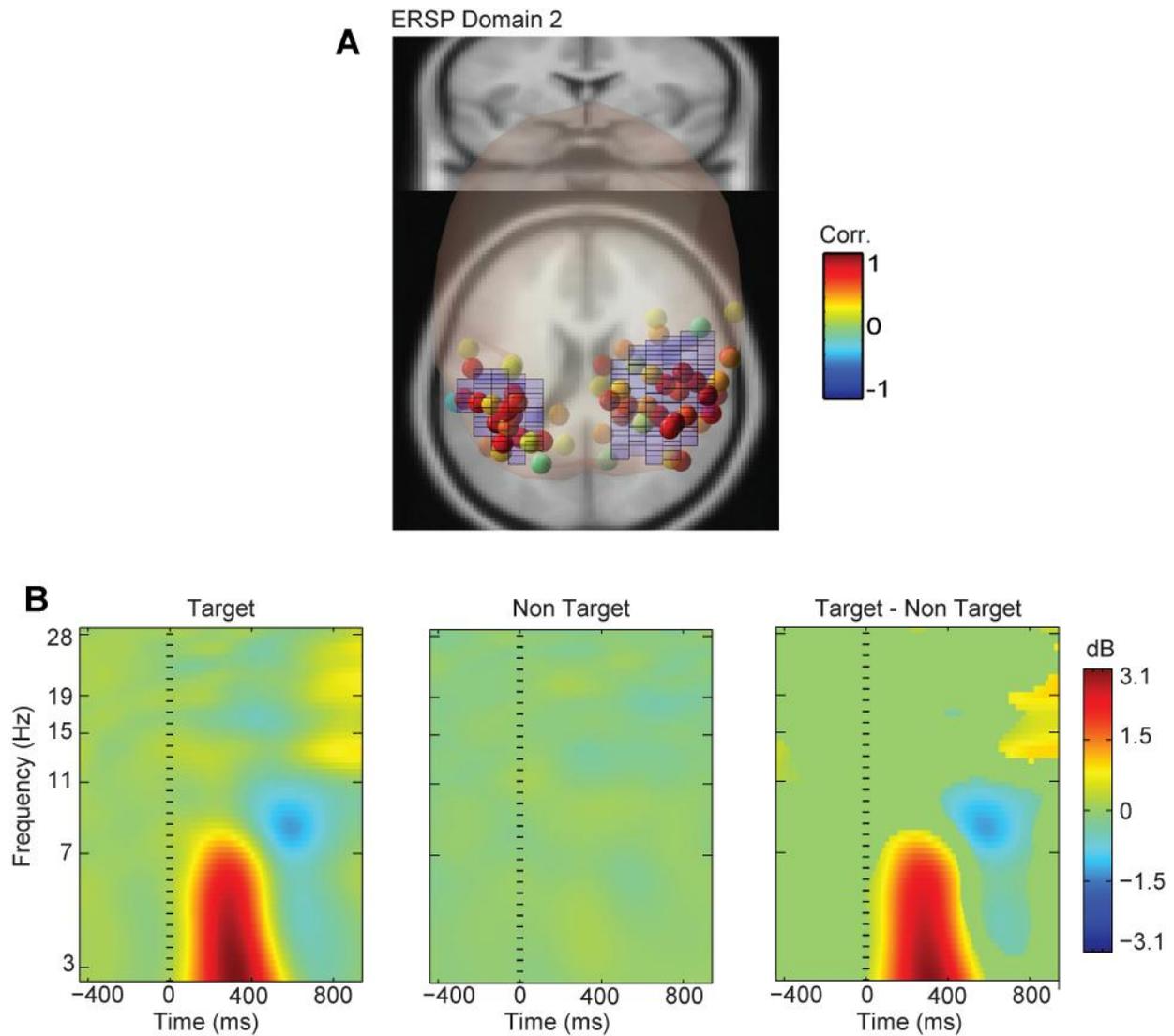
Fig. 8. **(A)** ERSP Domain 2 dipoles with probability of membership in the domain above 0.05 are colored by the correlation of the dipole-associated measure with the domain exemplar. **(B)** (left and center) Projected Target and Non-Target condition ERSPs for ERSP Domain 2, and (right) their statistically masked difference ($p<0.05$).
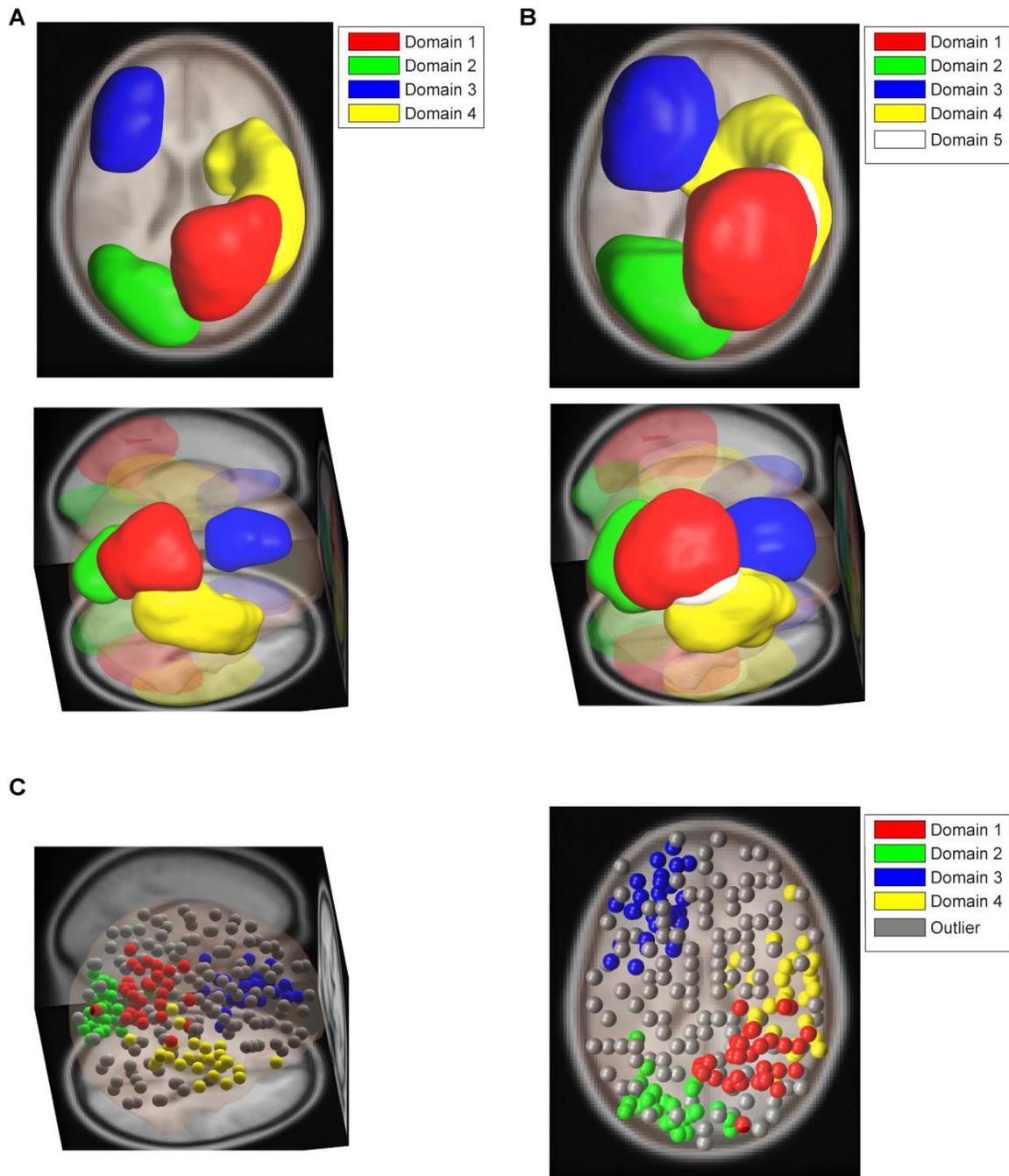
Fig. 9. **(A)** Simulated ground-truth domain set consisting of four anatomical regions **(B)** MPA results based on using 12-mm Gaussian spatial noise blurring and an 0.88 ERSP Signal-to-Noise Ratio (SNR). **(C)** Simulated dipoles including subsets associated with each ground-truth ERSP domain plus randomly located outliers given random ERSP measures.
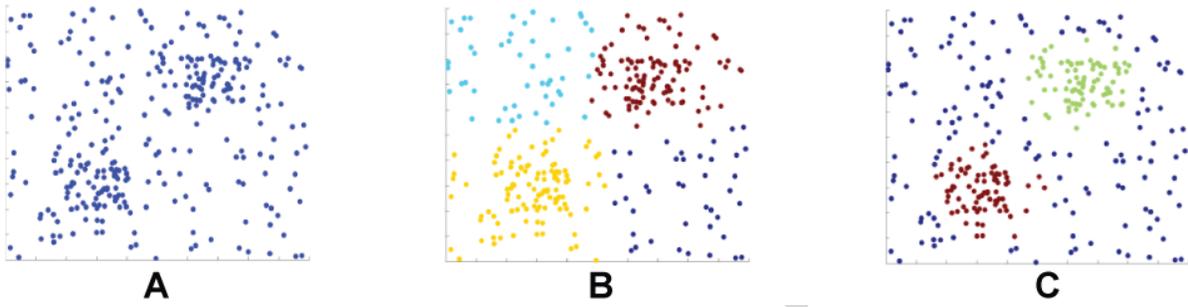
Fig. B.1. (A) Simulated sample points to illustrate Threshold-based clustering. (B) Points colored by cluster using $T_e = 0.2$ without outlier detection. (C) Points colored by cluster using $T_e = 0.2$ with outlier detection ($T_o = 0.2$).

References

Acar, Z.A., Makeig, S., 2010. Neuroelectromagnetic Forward Head Modeling Toolbox. Journal of Neuroscience Methods 190, 258-270.

Acar, Z.A., Worrell, G., Makeig, S., 2009. Patch-basis electrocortical source imaging in epilepsy. Engineering in Medicine and Biology Society, 2009. EMBC 2009. Annual International Conference of the IEEE, pp. 2930-2933.

Beckmann, C.F., Smith, S.M., 2005. Tensorial extensions of independent component analysis for multisubject FMRI analysis. NeuroImage 25, 294-311.

Bell, A.J., Sejnowski, T.J., 1995. An Information Maximization Approach to Blind Separation and Blind Deconvolution. Neural Computation 7, 1129-1159.

Benjamini, Y., Hochberg, Y., 1995. Controlling the False Discovery Rate - a Practical and Powerful Approach to Multiple Testing. Journal of the Royal Statistical Society Series B-Methodological 57, 289-300.

Bigdely-Shamlo, N., Vankov, A., Ramirez, R.R., Makeig, S., 2008. Brain Activity-Based Image Classification From Rapid Serial Visual Presentation. Ieee Transactions on Neural Systems and Rehabilitation Engineering 16, 432-441.

Brodmann, K., 1909. Vergleichende Lokalisationslehre der Grosshirnrinde. ihren Prinzipien dargestellt auf Grund des Zellenbaues.

Calhoun, V.D., Adali, T., Pearlson, G.D., Pekar, J.J., 2001. A method for making group inferences from functional MRI data using independent component analysis. Human Brain Mapping 14, 140-151.

Calhoun, V.D., Liu, J., Adali, T., 2009. A review of group ICA for fMRI data and ICA for joint inference of imaging, genetic, and ERP data. NeuroImage 45, S163-S172.

Cichocki, A., Amari, S.i., 2002. Adaptive blind signal and image processing : learning algorithms and applications. J. Wiley, Chichester ; New York.

Cohen, J., 1960. A Coefficient of Agreement for Nominal Scales. Educational and Psychological Measurement 20, 37-46.

Congedo, M., John, R.E., De Ridder, D., Prichep, L., 2010. Group independent component analysis of resting state EEG in large normative samples. International journal of psychophysiology : official journal of the International Organization of Psychophysiology 78, 89-99.

Darbellay, G.A., Vajda, I., 1999. Estimation of the information by an adaptive partitioning of the observation space. Ieee Transactions on Information Theory 45, 1315-1321.

Deary, I.J., Simonotto, E., Meyer, M., Marshall, A., Marshall, I., Goddard, N., Wardlaw, J.M., 2004. The functional anatomy of inspection time: an event-related fMRI study. NeuroImage 22, 1466-1479.

Delorme, A., Makeig, S., 2004. EEGLAB: an open source toolbox for analysis of single-trial EEG dynamics including independent component analysis. Journal of Neuroscience Methods 134, 9-21.

Delorme, A., Palmer, J., Onton, J., Oostenveld, R., Makeig, S., 2012. Independent EEG sources are dipolar. PloS one 7, e30135.

Dougherty, R.F., Koch, V.M., Brewer, A.A., Fischer, B., Modersitzki, J., Wandell, B.A., 2003. Visual field representations and locations of visual areas V1/2/3 in human visual cortex. Journal of Vision 3, 586-598.

Eichele, T., Calhoun, V.D., Debener, S., 2009. Mining EEG-fMRI using independent component analysis. International Journal of Psychophysiology 73, 53-61.

Esposito, F., Scarabino, T., Hyvarinen, A., Himberg, J., Formisano, E., Comani, S., Tedeschi, G., Goebel, R., Seifritz, E., Di Salle, F., 2005. Independent component analysis of fMRI group studies by self-organizing clustering. NeuroImage 25, 193-205.

Evans, A.C., Collins, D.L., Mills, S.R., Brown, E.D., Kelly, R.L., Peters, T.M., 1993. 3D statistical neuroanatomical models from 305 MRI volumes. Nuclear Science Symposium and Medical Imaging Conference, 1993., 1993 IEEE Conference Record., pp. 1813-1817 vol.1813.

Friston, K.J., 2007. Statistical parametric mapping : the analysis of funtional brain images, 1st ed. Elsevier/Academic Press, Amsterdam ; Boston.

Gerson, A.D., Parra, L.C., Sajda, P., 2005. Cortical origins of response time variability during rapid discrimination of visual objects. NeuroImage 28, 342-353.

Heller, R., Stanley, D., Yekutieli, D., Rubin, N., Benjamini, Y., 2006. Cluster-based analysis of FMRI data. NeuroImage 33, 599-608.

Hyvarinen, A., 2011. Testing the ICA mixing matrix based on inter-subject or inter-session consistency. NeuroImage 58, 122-136.

Jung, T.P., Makeig, S., McKeown, M.J., Bell, A.J., Lee, T.W., Sejnowski, T.J., 2001. Imaging brain dynamics using independent component analysis. Proceedings of the Ieee 89, 1107-1122.

Kiebel, S.J., Friston, K.J., 2004. Statistical parametric mapping for event-related potentials: I. Generic considerations. NeuroImage 22, 492-502.

Kovacevic, N., McIntosh, A.R., 2007. Groupwise independent component decomposition of EEG data and partial least square analysis. NeuroImage 35, 1103-1112.

Lancaster, J.L., Woldorff, M.G., Parsons, L.M., Liotti, M., Freitas, E.S., Rainey, L., Kochunov, P.V., Nickerson, D., Mikiten, S.A., Fox, P.T., 2000. Automated Talairach Atlas labels for functional brain mapping. Human Brain Mapping 10, 120-131.

Lee, T.W., Girolami, M., Sejnowski, T.J., 1999. Independent component analysis using an extended infomax algorithm for mixed subgaussian and supergaussian sources. Neural Computation 11, 417-441.

Li, X.L., Adali, T., Anderson, M., 2011. Joint blind source separation by generalized joint diagonalization of cumulant matrices. Signal Processing 91, 2314-2322.

Li, Y.O., Adali, T., Wang, W., Calhoun, V.D., 2009. Joint Blind Source Separation by Multi-set Canonical Correlation Analysis. IEEE transactions on signal processing : a publication of the IEEE Signal Processing Society 57, 3918-3929.

Makeig, S., 1993. Auditory Event-Related Dynamics of the Eeg Spectrum and Effects of Exposure to Tones. Electroencephalography and Clinical Neurophysiology 86, 283-293.

Makeig, S., Bell, A.J., Jung, T.P., Sejnowski, T., 1996. Independent component analysis of electroencephalographic data. Advances in Neural Information Processing Systems 8, 145-151

Makeig, S., Delorme, A., Westerfield, M., Jung, T.P., Townsend, J., Courchesne, E., Sejnowski, T.J., 2004. Electroencephalographic brain dynamics following manually responded visual targets. Plos Biology 2, 747-762.

Makeig, S., Jung, T.P., 1995. Changes in alertness are a principal component of variance in the EEG spectrum. Neuroreport 7, 213-216.

Makeig, S., Jung, T.P., Bell, A.J., Ghahremani, D., Sejnowski, T.J., 1997. Blind separation of auditory event-related brain responses into independent components. Proceedings of the National Academy of Sciences of the United States of America 94, 10979-10984.

Makeig, S., Westerfield, M., Jung, T.P., Enghoff, S., Townsend, J., Courchesne, E., Sejnowski, T.J., 2002. Dynamic brain sources of visual evoked responses. Science 295, 690-694.

Marcar, V.L., Loenneker, T., Straessle, A., Jaggy, S., Kucian, K., Martin, E., 2004. An fMRI study of the cerebral macro network involved in 'cue invariant' form perception and how it is influenced by stimulus complexity. NeuroImage 23, 947-955.

Maris, E., Oostenveld, R., 2007. Nonparametric statistical testing of EEG- and MEG-data. Journal of Neuroscience Methods 164, 177-190.

Mognon, A., Jovicich, J., Bruzzone, L., Buiatti, M., 2011. ADJUST: An automatic EEG artifact detector based on the joint use of spatial and temporal features. Psychophysiology 48, 229-240.

Moosmann, M., Eichele, T., Nordby, H., Hugdahl, K., Calhoun, V.D., 2008. Joint independent component analysis for simultaneous EEG-fMRI: Principle and simulation. International Journal of Psychophysiology 67, 212-221.

Nunez, P.L., Srinivasan, R., 2006. Electric fields of the brain : the neurophysics of EEG, 2nd ed. Oxford University Press, Oxford ; New York.

Onton, J., Makeig, S., 2006. Information-based modeling of event-related brain dynamics. Event-Related Dynamics of Brain Oscillations 159, 99-120.

Onton, J., Westerfield, M., Townsend, J., Makeig, S., 2006. Imaging human EEG dynamics using independent component analysis. Neuroscience and Biobehavioral Reviews 30, 808-822.

Oostenveld, R., Fries, P., Maris, E., Schoffelen, J.M., 2011. FieldTrip: Open source software for advanced analysis of MEG, EEG, and invasive electrophysiological data. Comput Intell Neurosci 2011, 156869.

Philiastides, M.G., Sajda, P., 2007. EEG-informed fMRI reveals spatiotemporal characteristics of perceptual decision making. J Neurosci 27, 13082-13091.

Picton, T.W., Bentin, S., Berg, P., Donchin, E., Hillyard, S.A., Johnson, R., Miller, G.A., Ritter, W., Ruchkin, D.S., Rugg, M.D., Taylor, M.J., 2000. Guidelines for using human event-related potentials to study cognition: Recording standards and publication criteria. Psychophysiology 37, 127-152.

Rachakonda, S., Eichele, T., Calhoun, V., 2011. Group ICA of EEG Toolbox (EEGIFT) Walk Through

Scherg, M., 1990. Fundamentals of dipole source potential analysis. In: Grandori, F., Hoke, M., Romani, G.L. (Eds.), Auditory evoked magnetic fields and electric potentials. Karger, Basel ; New York, pp. 40-69.

Schmithorst, V.J., Holland, S.K., 2004. Comparison of three methods for generating group statistical inferences from independent component analysis of functional magnetic resonance imaging data. Journal of Magnetic Resonance Imaging 19, 365-368.

Shattuck, D.W., Mirza, M., Adisetiyo, V., Hojatkashani, C., Salamon, G., Narr, K.L., Poldrack, R.A., Bilder, R.M., Toga, A.W., 2008. Construction of a 3D probabilistic atlas of human cortical structures. NeuroImage 39, 1064-1080.

Spadone, S., de Pasquale, F., Mantini, D., Della Penna, S., 2012. A K-means multivariate approach for clustering independent components from magnetoencephalographic data. NeuroImage.

Via, J., Anderson, M., Li, X.-L., Adali, T., 2011. Joint blind source separation from second-order statistics: Necessary and sufficient identifiability conditions. Acoustics, Speech and Signal Processing (ICASSP), 2011 IEEE International Conference on, pp. 2520-2523.

Viola, F.C., Thorne, J., Edmonds, B., Schneider, T., Eichele, T., Debener, S., 2009. Semi-automatic identification of independent components representing EEG artifact. Clinical Neurophysiology 120, 868-877.

Worsley, K.J., Taylor, J.E., Tomaiuolo, F., Lerch, J., 2004. Unified univariate and multivariate random field theory. NeuroImage 23 Suppl 1, S189-195.

Highlights
We introduce a novel statistical method for multi-subject EEG source analysis.

This method characterizes the spatial consistency of group EEG source dynamics.

Our method is an alternative to ICA clustering and has fewer parameters.

3-D maps with statistical significance estimates for EEG measures are produced.

The new method is validated on real and simulated EEG data.